Science of the Total Environment 607–608 (2017) 771–785

Contents lists available at ScienceDirect

Science of the Total Environment

journal homepage: www.elsevier.com/locate/scitotenv

Carbon dynamics in a Late Quaternary-age coastal limestone aquifer system undergoing saltwater intrusion

Eliza Bryan [a,b,c,*], Karina T. Meredith [b], Andy Baker [a,c], Martin S. Andersen [a,d], Vincent E.A. Post [e]

[a] Connected Waters Initiative Research Centre, UNSW Sydney, NSW 2052, Australia
[b] Australian Nuclear Science and Technology Organisation, Lucas Heights, NSW 2234, Australia
[c] School of Biological Earth and Environmental Sciences, UNSW Sydney, NSW 2052, Australia
[d] School of Civil and Environmental Engineering, UNSW Sydney, NSW 2052, Australia
[e] School of the Environment, Flinders University, GPO Box 2100, Adelaide, SA 5001, Australia

GRAPHICAL ABSTRACT

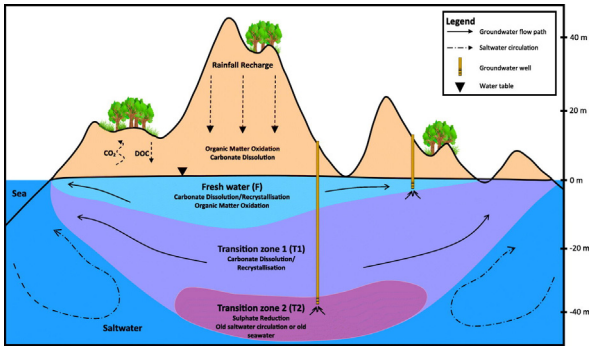

ARTICLE INFO

Article history:
Received 5 April 2017
Received in revised form 7 June 2017
Accepted 11 June 2017
Available online xxxx

Editor: D. Barcelo

Keywords:
Dissolved inorganic and organic carbon
Carbon isotopes
Radiocarbon
Recrystallisation
Seawater intrusion

ABSTRACT

This study investigates the inorganic and organic aspects of the carbon cycle in groundwaters throughout the freshwater lens and transition zone of a carbonate island aquifer and identifies the transformation of carbon throughout the system. We determined ^{14}C and ^{13}C carbon isotope values for both DIC and DOC in groundwaters, and investigated the composition of DOC throughout the aquifer. In combination with hydrochemical and ^{3}H measurements, the chemical evolution of groundwaters was then traced from the unsaturated zone to the deeper saline zone. The data revealed three distinct water types: Fresh (F), Transition zone 1 (T1) and Transition zone 2 (T2) groundwaters. The ^{3}H values in F and T1 samples indicate that these groundwaters are mostly modern. $^{14}C_{DOC}$ values are higher than $^{14}C_{DIC}$ values and are well correlated with ^{3}H values. F and T1 groundwater geochemistry is dominated by carbonate mineral recrystallisation reactions that add dead carbon to the groundwater. T2 groundwaters are deeper, saline and characterised by an absence of ^{3}H, lower $^{14}C_{DOC}$ values and a different DOC composition, namely a higher proportion of Humic Substances relative to total DOC. The T2 groundwaters are suggested to result from either the slow circulation of water within the seawater wedge, or from old remnant seawater caused by past sea level highstands. While further investigations are required to identify the origin of the T2 groundwaters, this study has identified their occurrence and shown that they did not evolve along the same pathway as fresh groundwaters. This study has also shown that a combined approach using ^{14}C and ^{13}C carbon isotope values for both DIC and DOC and the composition of DOC, as well as hydrochemical and ^{3}H measurements, can provide invaluable information regarding the transformation of carbon in a groundwater system and the evolution of fresh groundwater recharge.

* Corresponding author.
E-mail address: eliza.bryan@unsw.edu.au (E. Bryan).

http://dx.doi.org/10.1016/j.scitotenv.2017.06.094
0048-9697/

1. Introduction

Estimating groundwater residence time is critical for our understanding of hydrogeological systems, for groundwater resource assessments and for the sustainable management of groundwater resources (Cartwright et al., 2013; Fan, 2016; Meredith et al., 2016). Understanding the age of groundwater resources in a coastal setting which are susceptible to seawater intrusion and often utilised as a potable water source is particularly important. In this setting, radioactive isotopes such as radiocarbon (^{14}C) and tritium (^{3}H), which are produced by the interaction of atmospheric gases with cosmic radiation, are the most commonly used tools to determine groundwater residence times (Clark and Fritz, 1997; Kalin, 2000; Edmunds, 2009). While ^{3}H is considered a robust tool for residence time calculations, it only covers a short time scale (<50 years). ^{14}C is suitable for longer time scales, but has many more problems associated with its application due to the cycling of carbon, especially in a coastal limestone aquifer. However, a suitable tracer for dating groundwater covering a similar age range as ^{14}C remains unavailable, leaving ^{14}C as the only option at present. As such, it is important to understand the carbon isotopic composition of Dissolved Inorganic Carbon (DIC; $^{14}C_{DIC}$, $\delta^{13}C_{DIC}$) and Dissolved Organic Carbon (DOC; $^{14}C_{DOC}$, $\delta^{13}C_{DOC}$) and how various carbon sources impact on $^{14}C_{DIC}$ and $^{14}C_{DOC}$ groundwater values. A key process that influences $^{14}C_{DIC}$ values involves the dissolution of old ^{14}C-free solid carbonates in the aquifer matrix (Munnich, 1957; Ingerson and Pearson, 1964), which dilutes the initial surface derived ^{14}C activity in the DIC pool and results in an apparent "aging" of groundwaters. Other processes which affect the $^{14}C_{DIC}$ activity include precipitation of the atmospheric DIC component, isotope exchange reactions between the carbonate phases, groundwater mixing and microbial respiration (Pearson and White, 1967; Pearson and Hanshaw, 1970; Mook, 1980; Murphy et al., 1989b).

The carbon sources in coastal aquifers include organic and inorganic carbon contributed from both marine and continental sediments (Yechieli et al., 2001). Not only can geochemical reactions affect the carbon isotopes but the physical process of mixing between different water bodies with varying chemistry can result in a mixture of waters with distinctly different residence times. The mixing of fresh groundwater and seawater may also promote additional geochemical reactions that directly (e.g. sulphate reduction, mixing corrosion) or indirectly (e.g. ion exchange) change the DIC content and its isotopic signature. High salinity waters may also complicate the interpretation of ^{14}C ages, as the salinity may influence the rate of isotopic exchange between solid calcium carbonate and dissolved bicarbonate ions (Wendt, 1971). A small number of studies have investigated the application of $^{14}C_{DIC}$ in coastal settings undergoing seawater intrusion (De Breuck and De Moor, 1991; Hahn, 1991; Yechieli et al., 2001; Sivan et al., 2004), where it has assisted in the identification of both modern and old seawater intrusion, as well as the rate of seawater intrusion.

The geochemical processes controlling the carbon mass balance of DIC are not complete without including those that involve DOC (Kalin, 2000), as the oxidation of DOC will contribute carbon to the groundwater DIC. DOC in groundwater originates from active biological processes in the soil, unsaturated and saturated zones, and may introduce fossil or modern organic material to the groundwater (Thurman, 1985a). The DOC may be derived from organic matter originating from decomposing organic carbon in the soil zone, which is produced by both C_3 (trees) and C_4 (grasses) photosynthetic pathways (Plummer and Sprinkle, 2001; Plummer and Glynn, 2013). When released as DOC it may be subsequently transported to the groundwater via recharge. Where organic matter comprises a significant input of carbon to a groundwater system, the isotopic composition of the source organic matter should be investigated (Kalin, 2000). Like $^{14}C_{DIC}$, $^{14}C_{DOC}$ will undergo exponential radioactive decay and can be used as a suitable tracer for estimating groundwater residence times and ages, provided only one DOC source exists (Wassenaar et al., 1991b). As soil and dissolved humic substances are a polymeric mixture of young and old organic carbon, finite $^{14}C_{DOC}$ ages should not be considered absolute ages, rather they represent the 'mean apparent age' or mean residence time of the humic material mixture (Van Veen and Paul, 1978; Murphy et al., 1989b; Wassenaar et al., 1990a).

The analysis of $^{14}C_{DOC}$ has been investigated in a relatively small number of studies (Spiker and Rubin, 1975; Thurman, 1985a; Murphy et al., 1989a; Murphy et al., 1989b; Pettersson et al., 1989; Wassenaar et al., 1989; Wassenaar et al., 1990a; Wassenaar et al., 1990b; Purdy et al., 1992) to assist with the interpretation of $^{14}C_{DIC}$ results, however to the authors' knowledge, the application of $^{14}C_{DOC}$ in coastal aquifers is unique to this study. The combined interpretation of DIC and DOC and their isotopes is expected to lead to improved understanding of the evolution of groundwater, and better age estimates based on $^{14}C_{DIC}$. This paper aims to identify the sources of carbon in an island aquifer from the freshwater lens to the saline groundwater, and the processes that affect its cycling throughout the system, using a combined approach of ^{14}C and ^{13}C carbon isotope values of both DIC and DOC, the composition of groundwater DOC and ^{3}H measurements. It specifically aims to trace the geochemical evolution of waters from rainfall to fresh groundwater in the modern setting and identify key reactions taking place. It then aims to investigate processes in the transition zone of the aquifer to identify whether groundwaters of varying salinity have evolved under similar pathways to fresh groundwaters. Finally, this study aims to identify the occurrence of modern and old seawater intrusion into the freshwater lens.

2. Environmental setting

2.1. Geology and hydrogeology

Rottnest Island is located approximately 18 km off the coast of Perth in the south-west Western Australia region (Fig. 1A) and is ~10.5 km long and up to 4.5 km wide, with a maximum elevation of ~45 m Australian Height Datum (AHD). The island is composed of Pleistocene to mid-Holocene carbonate aeolianite (Tamala Limestone) with a total thickness of ~115 m (Playford and Leech, 1977). The Tamala Limestone on Rottnest Island varies from strongly lithified to friable and consists of creamy-white to yellow, or light-grey calcarenites which contains various proportions of quartz sand, fine- to medium-grained shell fragments, and minor clayey lenses (Playford et al., 1976). The calcarenites are composed of 50–99% fine to coarse sand-sized carbonate bioclasts (Playford et al., 1976; Mory, 1995; Playford, 1997; Hearty and O'Leary, 2008). The carbonate composition is assumed to be similar to that of the mainland Tamala Limestone Grey member, which is comprised of approximately 21% aragonite, 12% high Mg-calcite and 67% low Mg-calcite (Lipar and Webb, 2014). The non-carbonate grains consist of quartz and minor amounts of microcline and orthoclase feldspar, ilmenite, magnetite, garnet, amphibole and epidote (Bastian, 1996; Lipar and Webb, 2015).The surficial geology is also composed of various sands, clay, silt and coquina which is present around the coastline and hypersaline lakes as indicated by Fig. 1A.

The Tamala Limestone can be considered typical of Late Quaternary age coastal aeolianites that are related to Quaternary sea level change, and are widely distributed globally (Brooke, 2001; Vacher and Quinn, 2004; Hearty and O'Leary, 2008). Several Tamala Limestone exposures in south-west Western Australia and on Rottnest Island have been examined, which show dune, paleosol and shallow marine units. The paleosols, which generally contain higher proportions of quartz grains and clay than the surrounding calcarenites, represent periods of local stand-still in dune development and the concurrent formation of soil and establishment of vegetation (Playford and Leech, 1977; Lipar and Webb, 2014; Lipar and Webb, 2015). The Tamala Limestone was previously dated by Hearty (2003) using whole-rock amino-acid racemisation, which revealed that the limestone was deposited in stages, commencing during Marine Isotope Stage (MIS) 5e, continuing

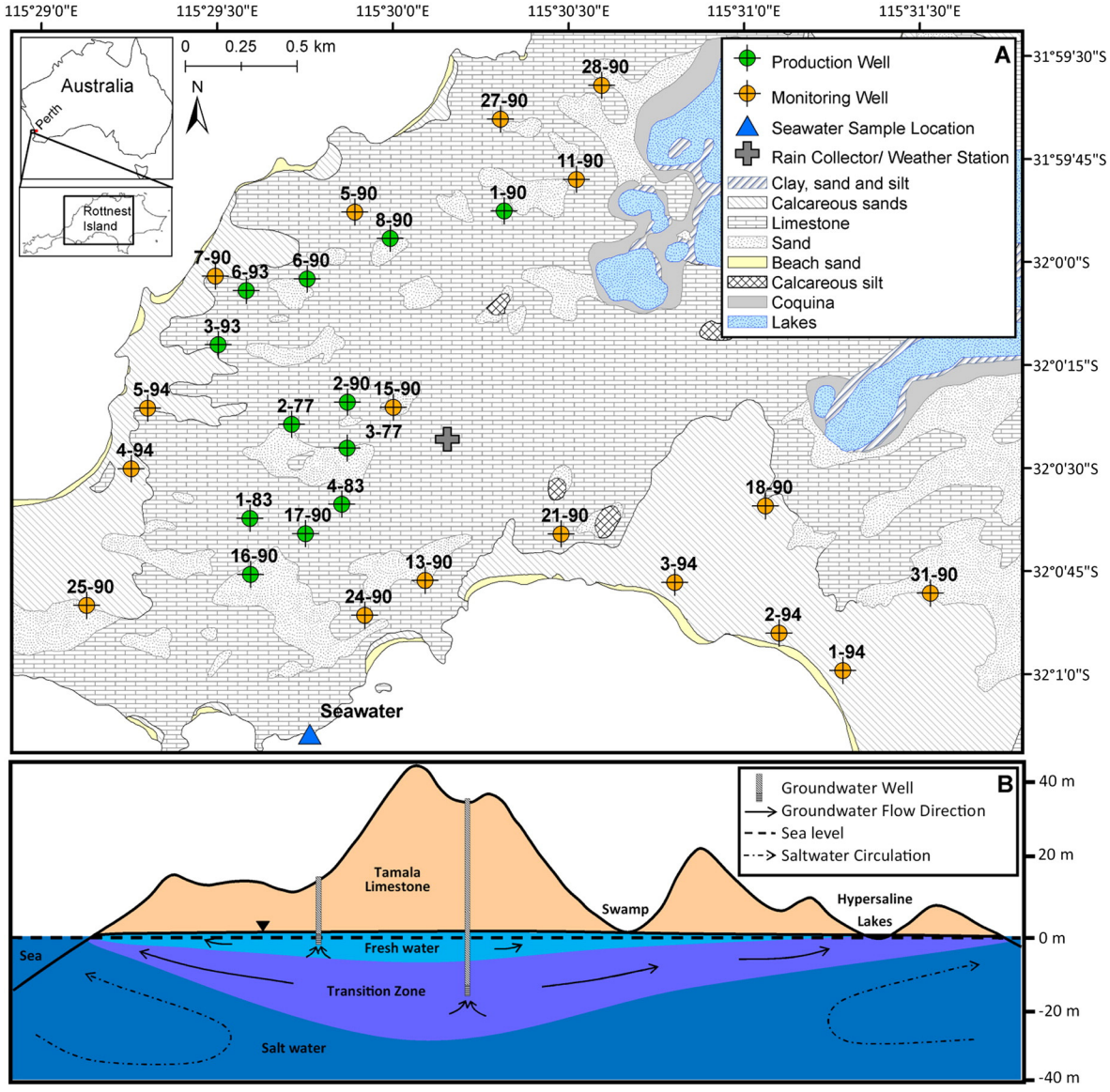

Fig. 1. A) Location and geological map of the study area showing sample locations (production and monitoring wells), weather station and rainfall collector. Surficial geology is based on information provided by Gozzard (2011); and **B**) A conceptual east-west cross section of Rottnest Island, adapted from Smith (1985), showing groundwater flow directions (Bryan et al., 2016). The numbers in Fig. 1A refer to well numbers.

through MIS 5c and peaking at the end of MIS 5a, approximately 70–80 ka ago (Hearty, 2003). As a result, the carbonate units within the Tamala Limestone are classified as "dead" with regards to ^{14}C and can be considered to have a value of 0 pMC. A study by Meredith et al. (2012) analysed two carbonate containing sediment samples for $\delta^{13}C$ composition from the top 25 m of a Tamala Limestone profile in the Perth Basin, which is in relatively close proximity to Rottnest Island. Results showed an enriched signature with an average $\delta^{13}C$ value of −1.0‰ (Meredith et al., 2012), which is typical of marine derived carbonate values (≈0‰; Craig, 1953).

Interbedded aeolian and paleosol sequences such as those observed on Rottnest Island are typical of Quaternary coastal sequences globally (Mauz et al., 2013; Pedoja et al., 2014; Rowe and Bristow, 2015; Swezey et al., 2016) and record complex cycles of coastal sedimentation linked to a wide range of sea-level positions and climatic periods of the middle and late Pleistocene (Fairbridge and Teichert, 1953; Playford et al., 1976; Kendrick et al., 1991; Brooke, 2001; Price et al., 2001; Hearty, 2003; Gozzard, 2007; Hearty and O'Leary, 2008; Playford et al., 2013; Brooke et al., 2014). Coshell and Rosen (1994) reported a sea level highstand, where sea level was ~2 m higher than present ~7 ka ago, while a study by Gouramanis et al. (2012) used an ostracod record in a sediment core from Barker Swamp on Rottnest Island to determine that a notable sea level highstand occurred between ~4.5 and 4.3 ka ago, which would have resulted in the incursion of marine water below the island and through the islands porous calcium carbonate sediment (Gouramanis et al., 2012).

Undulating sand dune hills characterise most of the island, with an absence of water courses due to the highly permeable nature of the Tamala Limestone. The island is similar to other carbonate aeolianite islands such as Bermuda and the Bahamas, which are all characterised by dune shaped topography, large amplitude, high-angle cross-bedding, paleosols and fossiliferous marine units (Vacher, 1997). A number of permanent hypersaline lakes at or slightly below mean sea level are present and cover approximately 10% of the Island's surface area (Playford and Leech, 1977), as well as many lower salinity inter-dunal swamps (Edward and Watson, 1959; Edward, 1983). The freshwater lens on the island is located within the upper section of the Tamala Limestone (Fig. 1B). The aquifer at all locations and depths is aeolianite and overlain by unconsolidated dune material in places. Thin paleosol sequences are also present. A transition zone below the fresh

groundwater is reported to be >10 m thick (Edward and Watson, 1959; Playford and Leech, 1977). The water table was previously documented to be at a maximum of ~0.5 m above sea level, with groundwater flowing from the centre of the lens towards the coast and hypersaline lakes (Bryan et al., 2016). Isotopic investigations showed that the hypersaline lakes had no impact on the composition of groundwaters that were previously sampled (Bryan et al., 2016). The spatial extent of the freshwater lens was reported to have contracted significantly since the late 1970s due to a decline in precipitation since the mid-1960s (Bryan et al., 2016), which has resulted in the rising of the transition zone and salinisation of fresh groundwaters, particularly in the northern area of the lens (Bryan et al., 2016).

2.2. Climate

Rottnest Island has a Mediterranean type climate characterised by hot, dry summers and mild, wet winters. The island has a long term average rainfall of 691 mm/year (1880–2015) and an annual reference evapotranspiration (ET_o) of 1694 mm (Station Number 9038 and 9193) (BOM, 2016).

2.3. Land use and vegetation

Rottnest Island has been used for various purposes since European settlement in the 1830s including as an aboriginal prison, for military training and agricultural production. In recent decades, it has primarily been a tourist destination. The native vegetation of Rottnest Island, which once covered an estimated 65% of the Island, has been heavily decimated by human activities and fire, with native forest and woodland cover reduced to 23% by 1941 and 5% by 1997 (Playford, 1997). The vegetation has been negatively impacted by native marsupials known as quokkas (*Setonix brachyurus*) (Rippey and Hobbs, 2003), with the reestablishment of native vegetation, particularly after fire, hindered by quokka grazing. The native flora of Rottnest Island consists of around 140 species, with the coast dominated by grasses including *Spinifex sericeus* and *Westringia fruticosa* (Gouramanis et al., 2012). *Acacia rostelifera* shrubs and three tree species (*Melaleuca lanceolata*, *Callitris preissii* and *Pittosporum ligustrifolium*) dominate the inland areas of the island (Rippey and Hobbs, 2003). Revegetation has commenced around the island, however the area above the freshwater lens has been left generally free of trees to ensure maximum recharge to the freshwater lens.

3. Methods

3.1. Field procedures

During two field campaigns in September 2014 and March 2015, twenty-nine samples were collected from production and monitoring wells throughout the study area (Fig. 1A). Samples were collected at, or just above the well screen, which is located at the bottom of each well, and measure a maximum of 1.5 m in length. The short screen length of both monitoring and production wells ensure a representative sample from varying depths throughout the aquifer. Prior to sampling, standing water levels were recorded and in-field measurements including pH, temperature, electrical conductivity (EC) and dissolved oxygen (DO) were measured (YSI 556 Multiparameter Instrument). Monitoring well samples were collected using a plastic submersible centrifugal pump (Supernova 120) after wells were purged of three well-volumes and stabilisation of in-field parameters was observed. Production well samples were collected using permanently installed pumps after purging until stabilisation of in-field parameters. One seawater sample was also collected using a peristaltic pump (Masterflex E/S portable sampler). Total alkalinity concentrations were determined by a double end-point titration method using a HACH digital titrator at a dedicated field laboratory at the end of each day.

Samples for anions, ^{3}H and $^{14}C_{DIC}$ analysis were filtered through 0.45 μm filters and collected in 60 mL and 1 L high density poly-ethylene (HDPE) bottles respectively, with no further treatment. Samples for cations were filtered through 0.45 μm filters and collected in 60 mL HDPE bottles and acidified with 65% Suprapur® nitric acid. Liquid Chromatography-Organic Carbon Detection (LC-OCD) samples were filtered through 0.45 μm filters, collected in 30 mL HDPE bottles and refrigerated until analysis. Stable isotopes of DIC ($^{13}C_{DIC}$) samples were filtered through 0.2 μm filters, collected in 12 mL glass vials (Exetainers) and refrigerated after sampling. Dissolved Organic Carbon (DOC) and stable isotopes of DOC ($^{13}C_{DOC}$) samples were filtered through 0.2 μm filters, collected in 60 mL HDPE bottles and frozen after sampling. $^{14}C_{DOC}$ samples were filtered through 0.2 μm filters, collected in 2 L HDPE bottles and frozen after sampling. All samples were sealed with tape after collection to limit atmospheric exchange.

Composite rainfall samples were collected on a weekly basis from May 2014–March 2015 in a rainfall collector designed to collect samples for isotopic analysis by preventing evaporation (Gröning et al., 2012). Samples for major ions were collected in 30 mL HDPE bottles, and sealed with tape after collection to limit atmospheric exchange. All samples were filtered, and samples for cations were acidified with 65% Suprapur® nitric acid, on return to the laboratory. In-field measurements were not collected, hence a pH value of 5.5 is assumed (Appelo and Postma, 2005).

3.2. Analysis

The chemical composition of water samples were analysed at the Australian Nuclear Science and Technology Organisation (ANSTO) by ion chromatography and inductively coupled plasma-atomic emission spectroscopy for anions and cations respectively. Analytical accuracy was assessed by evaluating the charge balance error, with 80% of the samples falling within ±5% and all samples falling within ±6.2%.

The $\delta^{13}C_{DIC}$ signatures of water samples were analysed at ANSTO by isotope ratio mass spectrometry (IRMS) and results were reported as per mil (‰) deviations from the international carbonate standard NBS19 ($\delta^{13}C = +1.95‰$ VPDB) with a precision of ±0.3‰. $^{13}C_{DOC}$ and DOC concentrations were analysed at the UC Davis Stable Isotope Facility using a total organic carbon analyser interfaced to a PDZ Europa20-20 IRMS utilising a GD-100 gas trap interface. $\delta^{13}C_{DOC}$ results were reported as per mil (‰) deviation from a standard reference material (KHP $\delta^{13}C = -25.17‰$ PDB) with an analytical precision of ±0.6‰. DOC characterisation was completed at the Mark Wainwright Analytical Centre at the University of New South Wales, Australia, and was based on methodology outlined by Huber et al. (2011). In brief, the analysis involves an automated size-exclusion chromatography system coupled to three detectors for organic carbon, organic nitrogen and UV absorbance, respectively. A Toyopearl HW-50S gel filtration column was used with a phosphate buffer mobile phase of pH 6.4 at a flow rate of 1.1 mL/min. Sample injection volumes were 1 mL. The chromatograms obtained were interpreted using the DOC-Labor ChromCALC software program, which identifies six fractions of DOC based on molecular weight; Humic Substances, Building Blocks, Biopolymers, Low Molecular Weight (LMW)-neutrals, LMW-acids and Hydrophobics (Refer to Table S1 - Supplementary Data for a description of each fraction (Huber et al., 2011, Rutlidge et al., 2015)).

$^{14}C_{DIC}$ and $^{14}C_{DOC}$ samples were analysed by accelerator mass spectrometry (AMS) at the ANSTO AMS facility described by Fink et al. (2004). The $^{14}C_{DIC}$ content of waters was determined by accelerator mass spectrometry after samples were processed according to the method outlined by Meredith et al. (2012). Briefly, the total DIC was converted into CO_2 by acidifying the samples and extracting the liberated CO_2 gas. The CO_2 sample was then heated with CuO, Ag and Cu wire at 600 °C for 2 h, followed by conversion into graphite by reducing it with excess hydrogen gas in the presence of an iron catalyst at 600 °C. $^{14}C_{DOC}$ samples were acidified to pH <2 with HCl, and rotary evaporated until approximately 95% of the sample water was removed. The sample

was transferred to a beaker and dried to completion, before the residue was heated with CuO, Ag and Cu wire at 600 °C for 2 h, followed by conversion into graphite as described above. The ^{14}C results from the laboratory were reported in percent Modern carbon (pMC) normalised against the $\delta^{13}C$ of the graphite, with an average 1σ error of the AMS readings at ±0.3 pMC. The 'un-normalised' $^{14}C_{DIC}$ values for groundwater were used and reported as pmc (Plummer and Glynn, 2013), which was calculated using the $^{14}C/^{12}C$ ratio and Eq. 1 provided by Mook and Van Der Plicht (1999). These values are used as the variation in groundwater $\delta^{13}C_{DIC}$ is caused by geochemical reactions that may affect $\delta^{13}C_{DIC}$ and $^{14}C_{DIC}$ differently, meaning that normalisation of the $^{14}C_{DIC}$ value against the graphite value would introduce additional error into the age calculations.

$$pmc = pMC\left[\left(\frac{1+{}^{13}\delta_{DIC}}{1000}\right)/0.975\right]^2 \quad (1)$$

^3H samples were analysed at ANSTO, with water samples distilled and electrolytically enriched prior to analysis by a liquid scintillation method. The ^3H concentrations were expressed in tritium units (TU) with a general uncertainty of ±0.1 TU and quantification limit of 0.06 TU.

The correlation of all results was calculated using a Spearman's Rank Correlation, to account for data that is not normally distributed.

3.3. Calculations

3.3.1. Ion enrichment and depletion

Reactions occurring in the transition zone can be revealed by comparing the measured water composition with the composition calculated for conservative mixing of freshwater and seawater. The fraction of seawater (f_{sea}) is calculated from the Cl^- concentration, assuming that it acts conservatively and that there is no additional source of Cl^- (Appelo and Postma, 2005):

$$f_{sea} = \frac{m_{Cl^-,sample} - m_{Cl^-,fresh}}{m_{Cl^-,sea} - m_{Cl^-,fresh}} \quad (2)$$

where $m_{Cl^-,sample}$, $m_{Cl^-,fresh}$ and $m_{Cl^-,sea}$ are the Cl^- concentrations in a sample, fresh groundwater and seawater respectively. The Cl^- concentration of the freshest groundwater sample (2-94), which was determined according to its low TDS value (474 mg/L), was used as the $m_{Cl^-,fresh}$ value.

The conservative mixing concentration ($m_{i,mix}$) for other dissolved species is then calculated from (Appelo and Postma, 2005):

$$m_{i,mix} = f_{sea} \cdot m_{i,sea} + (1 - f_{sea}) \cdot m_{i,fresh} \quad (3)$$

where $m_{i,sea}$ and $m_{i,fresh}$ are the concentrations in seawater and freshwater of the species *i*. The enrichment or depletion (m_{react}) of the species *i* is then obtained by (Appelo and Postma, 2005):

$$m_{react} = m_{i,sample} - m_{i,mix} \quad (4)$$

A positive m_{react} indicates that the groundwater is enriched for species *i*, and a negative m_{react} indicates that the groundwater is depleted for species *i*, compared to conservative mixing.

3.3.2. Hydrogeochemical interpretation and mass balance modelling

Saturation indices for calcite and aragonite, the partial pressure of CO_2 (pCO_2), HCO_3^- concentration, as well as DIC concentrations were calculated with the hydrogeochemical software PHREEQC 3, using the PHREEQC database (Parkhurst and Appelo, 2013). Calculations were made with field alkalinity and pH values.

The interactive computer code NETPATH (Plummer et al., 1991) was used to reconstruct mass balance reactions and quantify the geochemical processes that are consistent with the evolution of the water chemistry observed between two points along a flow path (inverse modelling), and was used to account for the cycling of carbon along conceptualised flow paths within the unsaturated zone and fresh groundwater on Rottnest Island. Modelling was based on the assumption that piston flow recharge is occurring in this system and that the groundwater system is at chemical steady state. All reactions observed were constrained by mass balance on Ca, Mg, C, and electron balance. Recrystallisation reactions were simulated by the dissolution of a high Mg-calcite (30 mol% Mg) with a $\delta^{13}C$ value of −1‰ and the precipitation of pure calcite in equilibrium with the groundwater $\delta^{13}C$ value. The proportion of Mg in High-Mg calcite was based on the maximum Mg mol% determined by other studies (Mucci, 1987, and references within). Each geochemical reaction model in NETPATH is solved as an isotope-evolution problem using Rayleigh distillation calculations (Wigley et al., 1978), which account for isotope fractionation along the flow path to predict the $\delta^{13}C_{DIC}$ isotopic composition of the final end member in the reaction. The modelled reactions can then be compared to measured $\delta^{13}C_{DIC}$ isotopic values, and the validity of the model assessed. Models that computed $\delta^{13}C_{DIC}$ values within ±1‰ of the measured value were considered. A more detailed description of this modelling approach is described by Plummer et al. (1991), Aravena et al. (1995) and Plummer and Sprinkle (2001).

4. Results

4.1. Inorganic chemistry

The groundwater hydrochemical and isotopic results from the Rottnest Island aquifer, along with one seawater sample and rainfall, are presented in Table 1. The rainfall composition on Rottnest Island is dominated by Na and Cl^-, and in general is characterised by low salinity, low DIC content and is assumed to have a pH of ~5.5 (Appelo and Postma, 2005).

A number of water types were found in the coastal aquifer (Bryan et al., 2016), which differ from each other by their salinity and chemical composition as determined by Fetter (2001): Fresh (<1000 mg/L TDS), Brackish (1000–10,000 mg/L TDS) and Saline (10,000–100,000 mg/L TDS). Ca concentrations range from 1.0–1.6 mmol/L in fresh groundwaters, from 1.3–3.9 mmol/L in brackish groundwaters and from 4.9–9.8 mmol/L in saline groundwaters (Fig. 2A). The Ca concentration in seawater is 10.4 mmol/L. Na concentrations range from 2.3–6.1 mmol/L in fresh groundwaters, from 7.3–93.7 mmol/L in brackish groundwaters and from 189.8–393.6 mmol/L in saline groundwaters. The Na concentration in seawater is 491.7 mmol/L. Mg concentrations range from 0.7–2.0 mmol/L in fresh groundwaters, from 2.0–10.6 mmol/L in brackish groundwaters and from 22.4–42.8 mmol/L in saline groundwaters. The Mg concentration in seawater is 55.5 mmol/L. Sr concentrations are below 0 mmol/L in fresh groundwaters, and range from 0–0.1 mmol/L in brackish groundwaters and from 0.1–0.3 mmol/L in saline groundwaters. The Sr concentration in seawater is 0.1 mmol/L. Cl^- concentrations range from 2.7–7.5 mmol/L in fresh groundwaters, from 8.8–97.4 mmol/L in brackish groundwaters and from 227.2–485.4 mmol/L in saline groundwaters. The Cl^- concentration in seawater is 573.4 mmol/L. HCO_3^- concentrations range from 3.4–5.1 mmol/L in fresh groundwaters, from 4.7–6.9 mmol/L in brackish groundwaters and from 2.6–4.1 mmol/L in saline groundwaters (Fig. 2B, C). The HCO_3^- concentration in seawater is 1.5 mmol/L. The sum of Ca and Mg show a positive correlation with HCO_3^- concentrations in the fresh and brackish groundwater ($r = 0.89$), however as the groundwater salinity increases further, HCO_3^- decreases as the sum of Ca and Mg increases ($r = -0.57$; Fig. 2C). The Mg/Ca molar ratio also increases with increasing $\delta^{13}C_{DIC}$ values ($r = 0.72$; Fig. 3).

SO_4^{2-} concentrations range from 0.3–0.7 mmol/L in fresh groundwaters, from 0.7–3.8 mmol/L in brackish groundwaters and from 11.3–23.6 mmol/L in saline groundwaters (Fig. S3A), while the SO_4^{2-}

Table 1
Hydrochemical and isotopic results for groundwaters, seawater and rainfall on Rottnest Island, as well as the mixing water type defined through the study.

Well ID	Sample type[a]	Sample date	Screen elevation	T[b]	pH	Field alkalinity	DO[c]	TDS[d]	Ca	Mg	Na	Sr	Fe_{TOT}[e]	Cl^-
			m AHD[m]	°C		mg/L $CaCO_3$	mg/L	mg/L	mmol/L	mmol/L	mmol/L	mmol/L	μmol/L	mmol/L
2-77	Prod	29/9/14	−0.11	18.45	7.64	225.7	1.78	672	1.0	1.7	4.2	0.0		4.5
3-77	Prod	29/9/14	−0.01	15.88	7.48	261.6	1.53	776	1.3	2.0	4.5	0.0		5.1
1-83	Prod	28/9/14	0.09	16.54	7.52	233.6	1.55	789	1.4	1.8	4.9	0.0		6.1
4-83	Prod	30/9/14	−0.11	16.79	7.78	216.8	4.23	674	1.0	2.0	3.8	0.0		4.4
1-90	Prod	29/9/14	−0.90	15.86	7.50	254.5	2.47	2461	1.9	3.8	26.4	0.1		35.1
2-90	Prod	29/9/14	−0.50	18.46	7.78	201.8	3.61	605	1.0	1.5	3.6	0.0		4.2
6-90	Prod	29/9/14	−0.64	18.64	7.66	232.4	3.39	799	1.5	1.6	5.4	0.0		6.7
8–90	Prod	29/9/14	−0.59	18.78	7.43	311.0	1.90	1144	1.5	2.6	8.9	0.0		9.2
16-90	Prod	28/9/14	−0.28	16.83	7.43	263.0	1.33	812	1.6	1.9	4.7	0.0		5.9
17-90	Prod	30/9/14	0.06	16.72	7.87	229.4	3.50	787	1.2	2.0	5.0	0.0		5.9
3-93	Prod	29/9/14	−0.27	18.68	7.59	210.0	2.92	833	1.2	2.0	6.1	0.0		7.5
6-93	Prod	29/9/14	−0.22	16.55	7.62	229.8	4.04	713	1.2	1.7	4.3	0.0		5.5
5-90	Mon	27/9/14	−6.90	17.33	7.33	377.5	0.35	6868	3.9	10.6	93.7	0.1		97.4
7-90	Mon	12/3/15	−7.06	22.25	7.44	185.0	3.26	20,676	6.9	31.9	279.4	0.1	0.3	325.5
11-90	Mon	26/9/14	−6.19	18.61	7.53	182.6	0.50	29,675	9.8	42.8	393.6	0.1	3.4	485.4
13-90	Mon	11/3/15	−3.55	20.10	7.15	197.5	0.50	4997	2.5	7.6	59.5	0.1		74.3
15-90	Mon	26/9/14	−14.92	19.42	7.52	154.5	0.15	22,977	7.3	33.4	287.2	0.3	3.1	386.8
18-90	Mon	27/9/14	−11.16	17.77	7.42	191.6	0.33	25,267	7.6	38.6	317.7	0.1		416.7
21-90	Mon	26/9/14	−4.04	19.13	7.36	325.0	0.32	3584	2.9	5.6	38.5	0.0	1.8	46.4
24-90	Mon	26/9/14	−3.47	19.43	7.56	275.6	0.38	1211	1.5	2.6	9.0	0.0	2.0	11.9
25-90	Mon	27/9/14		17.52	7.54	208.6	0.29	14,489	4.9	22.4	189.8	0.1		227.2
27-90	Mon	26/9/14	−4.98	18.96	7.29	244.8	0.86	20,824	7.1	32.8	293.2	0.1		314.0
28-90	Mon	26/9/14	−1.52	19.96	7.47	245.7	1.07	1986	2.2	2.6	20.6	0.0		27.4
31-90	Mon	28/9/14	−9.20	18.40	7.62	205.2	0.28	16,344	7.8	25.9	219.8	0.1		247.2
1-94	Mon	28/9/14	−0.53	18.73	7.71	231.4	4.64	667	1.5	1.3	3.7	0.0		4.5
2-94	Mon	28/9/14	−1.00	19.17	7.60	176.7	7.05	474	1.5	0.7	2.3	0.0		2.7
3-94	Mon	27/9/14	−0.72	17.56	7.55	251.3	3.04	1244	1.8	2.0	10.8	0.0		13.7
4-94	Mon	27/9/14	−1.83	17.47	7.63	287.2	2.41	1075	1.4	2.8	7.3	0.0		8.9
5-94	Mon	27/9/14	−1.87	18.58	7.70	252.7	1.13	1040	1.3	2.6	7.5	0.1		8.8
SW	SW	12/3/15	0.00	21.19	8.13	109.8	6.69	35,780	10.4	55.5	491.7	0.1		573.4
RF	RF				5.50[r]				0.12	0.20	1.78	0.0		2.13
RF[t]	RF								0.15	0.25	2.25	0.0		

[a] Prod = Production well, Mon = Monitoring well, SW = Seawater, RF = rainfall.
[b] Temperature.
[c] Dissolved Oxygen.
[d] Total Dissolved Solids.
[e] Total Iron.
[f] Charge Balance Error.
[g] Saturation Indices for Calcite.
[h] Saturation Indices for Aragonite.
[i] Partial Pressure of CO_2.
[j] Dissolved Inorganic Carbon.
[k] Dissolved Organic Carbon.
[l] F = Fresh groundwater, T1 = Transition zone 1 groundwater, T2 = Transition zone 2 groundwater.
[m] Meters Australian Height Datum.
[n] Atmosphere.
[o] Percent modern carbon.
[p] Percent Modern Carbon (normalised).
[q] Tritium Units.
[r] Assumed value.
[s] Calculated by difference.
[t] Concentration factor of 1.3 applied.

Table 1 *(continued)*

SO_4^{2-}	NO_3^-	HCO_s^-	CBE[f]	SI_{cc}[g]	SI_{Ar}[h]	P_{CO2}[i]	DIC[j]	$\delta^{13}C_{DIC}$	$^{14}C_{DIC}$	DOC[k]	$\delta^{13}C_{DOC}$	$^{14}C_{DOC}$	^3H	Mixing type[l]
mmol/L	mmol/L	mmol/L	%			atm[n]	mmol/L	‰	pmc[o]	mg/L	‰	pMC[p]	TU[q]	
0.5	0.1	4.4	−2.1	0.08	−0.07	0.005	4.7	−7.0	52.50	1.18	−24.96		0.93	F
0.7	0.2	5.1	−2.6	0.02	−0.13	0.009	5.6	−8.2	56.64	1.13	−25.01	88.91	0.89	F
0.6	0.2	4.5	−3.8	0.05	−0.10	0.007	5.0	−8.6	66.53	1.96	−24.66	105.62	0.96	F
0.7	0.3	4.2	−2.7	0.18	0.03	0.004	4.5	−5.9	45.32	1.24	−25.28		1.11	F
1.0	0.3	4.9	−5.0	0.06	−0.09	0.007	5.4	−6.7	48.50	1.40	−26.92	54.46		T1
0.4	0.2	3.9	−2.9	0.18	0.03	0.003	4.2	−6.5	41.81	0.56	−26.51		0.87	F
0.5	0.2	4.5	−3.8	0.25	0.10	0.005	4.8	−8.6	67.68	1.02	−26.26		0.62	F
1.0	0.7	6.0	−2.5	0.10	−0.05	0.012	6.7	−7.3	56.81	2.02	−25.86	97.50		T1
0.5	0.2	5.1	−2.8	0.08	−0.07	0.010	5.7	−9.8	74.13	2.90	−26.09	99.78	0.96	F
0.7	0.3	4.4	−3.1	0.32	0.17	0.003	4.7	−8.6	66.12	1.53	−25.49	93.73		F
0.7	0.3	4.1	−3.1	0.03	−0.12	0.006	4.4	−5.9	44.45	0.83	−25.99			F
0.4	0.2	4.5	−5.1	0.09	−0.06	0.006	4.8	−5.8	46.39	0.78	−26.58			F
3.3	0.4	6.9	5.5	0.22	0.07	0.015	8.2	−2.3	8.71	1.20	−26.27		0.12	T2
16.6	0.1	3.1	−0.03	0.12	−0.03	0.005	3.9	−3.1	21.17	0.10	−30.30		0.67	T1
23.6		2.9	−2.9	0.25	0.10	0.004	3.8	−7.3	43.98	1.10	−24.84	57.78	0.09	T2
2.9	0.5	6.0	−3.75	−0.12	−0.27	0.021	7.2	−4.1	23.99	1.00	−28.60		0.21	T1
16.4		2.6	−6.2	0.10	−0.05	0.003	3.2	−2.9	8.35	0.50	−25.51		0.03	T2
20.8	0.2	3.1	−5.3	0.06	−0.08	0.005	4.1	−5.9	35.12	0.20	−23.87	50.61	0.07	T2
3.8	0.0	6.1	−3.4	0.18	0.03	0.013	7.0	−9.0	59.33	2.80	−25.90	91.48	0.62	T1
1.1		5.3	−5.8	0.19	0.04	0.008	5.8	−7.4	56.31	2.20	−24.83	94.80	0.65	T1
11.3	0.1	3.6	−1.2	0.13	−0.02	0.004	4.4	−2.2	13.18	0.20	−27.07	46.57	0.04	T2
17.8	0.3	4.1	3.4	0.06	−0.09	0.009	5.3	−3.0	18.28	0.40	−26.03	66.99	0.29	T2
0.7	0.3	4.7	−4.9	0.18	0.03	0.008	5.2	−9.8	77.03	0.80	−26.59	83.97	0.95	T1
14.4	0.1	3.4	2.0	0.38	0.23	0.004	4.2	−9.4	52.47	0.90	−31.07	66.93	0.07	T2
0.4	0.2	4.5	−2.7	0.34	0.19	0.005	4.8	−9.7	85.76	0.60	−25.24		1.16	F
0.3	0.1	3.4	−1.8	0.14	−0.01	0.005	3.7	−11.0	95.23	0.60	−25.33		1.35	F
0.7	0.1	4.8	−4.0	0.20	0.05	0.007	5.3	−11.4	97.21	0.80	−26.61		1.04	T1
1.0	0.4	5.5	−3.8	0.23	0.08	0.007	6.0	−6.7	54.68	1.30	−25.44		0.67	T1
1.2	0.3	4.9	−2.8	0.22	0.07	0.005	5.2	−4.1	28.23	0.90	−24.66	86.11	0.42	T1
32.1	0.0	1.5	−0.52	0.60	0.45	0.000	0.0	0.9		0.40	−24.50			
0.14		0.05[s]												
0.17														

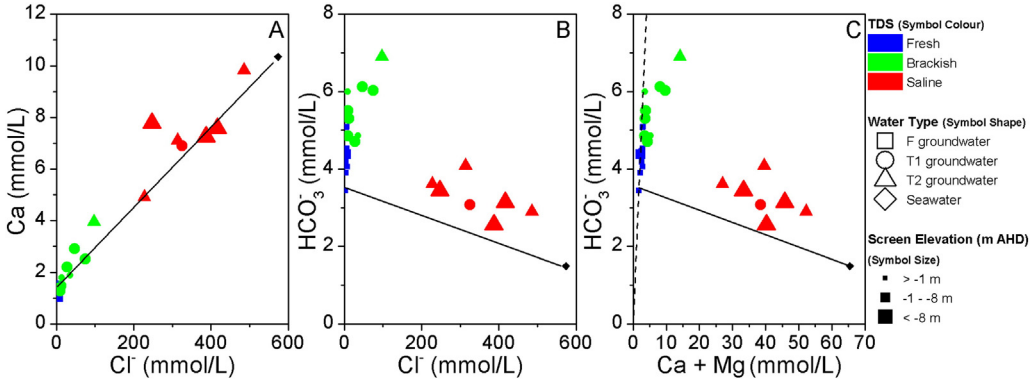

Fig. 2. Bivariate plots of A) Ca vs. Cl^-, B) HCO_3^- vs. Cl^- and C) HCO_3^- vs. Ca + Mg in groundwaters. Fig. 2C shows a 2:1 (HCO_3^-:Ca + Mg) ratio (dashed line) and all figures show a conservative mixing line (solid line) between a freshwater and seawater end-member. Samples are grouped according to the TDS classification (Fresh: <1000 mg/L, Brackish: 1000–10,000 mg/L, Saline: 10,000–100,000 mg/L) outlined by Fetter (2001) and symbol size according to screen elevation.

concentration in seawater is 32.1 mmol/L. SO_4^{2-} values are well correlated with Cl^- ($r = 0.93$) and the data points follow a conservative mixing line between fresh groundwater and seawater (Fig. S3A). NO_3^- is present in most groundwaters, with concentrations ranging from 0.1–0.3 mmol/L in fresh groundwaters, from 0.0–0.7 mmol/L in brackish groundwaters and from 0.1–0.3 mmol/L in saline groundwaters (Fig. S3B). NO_3^- concentrations do not show a strong correlation with Cl^- ($r = -0.17$; Fig. S3B) and the NO_3^- concentration in seawater is below detection limits. Total Fe concentrations were below detection limits in all fresh groundwater samples and most brackish and saline samples, however five samples had measurable Fe concentrations that ranged from 0.3–3.4 μmol/L (Table 1). DO concentrations ranged from 1.3–7.0 mg/L in fresh groundwaters, from 0.3–3.0 mg/L in brackish groundwaters and from 0.1–3.3 mg/L in saline groundwaters and decrease with increasing Cl^- concentration ($r = -0.74$; Fig. S3C) and decreasing screen elevation ($r = 0.68$). All groundwaters (except one) are in equilibrium or slightly oversaturated with respect to calcite (Fig. S3D) and most groundwaters are close to saturation with respect to aragonite (Table 1).

Ionic exchange reactions occurring in the aquifer were investigated by comparing the measured water composition with the expected water composition resulting from the conservative mixing of freshwater and seawater (Eqs. (2)–(4)). Results are shown in Table S2 and bivariate plots of m_{react} values vs. elevation are shown in Fig. S4. Over half of the groundwaters show a deficit of Ca compared to conservative mixing ($Ca_{react} < 0$; Fig. S4A), with freshwater Ca_{react} values ranging from −0.5 to 0.1 mmol/L, brackish values from −0.3 to 1.0 mmol/L and saline values from −0.3 to 2.5. An excess of Mg ($Mg_{react} > 0$) is observed in all fresh waters ($Mg_{react} = 0.5$–1.1 mmol/L) and all but one brackish groundwater (−0.5–1.5 mmol/L), while a deficit is noted in most saline groundwaters (−4.2–2.3 mmol/L; Fig. S4A). Most fresh samples show a small deficit in Na ($Na_{react} < 0$), with Na_{react} values ranging from −0.4 to 0.4 mmol/L. Brackish and saline Na_{react} values show more variation and range from −4.2 to 10.2 mmol/L and −44.6 to 23.9 mmol/L respectively (Fig. S4B). All samples show an excess of HCO_3^- ($HCO_3^-{}_{react} > 0$) compared to conservative mixing, with $HCO_3^-{}_{react}$ values ranging from 0.4 to 3.8 mmol/L (Fig. S4C). Brackish groundwaters show the highest excess of HCO_3^-, which ranges from 1.3 to 3.8 mmol/L, compared with 0.5–1.7 mmol/L for fresh and 0.4–1.7 mmol/L for saline groundwaters (Fig. S4C). Around half of the groundwater samples showed a deficit of SO_4^{2-} compared to conservative mixing ($SO_4^{2-}{}_{react} < 0$), with the largest deficit observed in brackish and saline samples which range from −2.2 to 1.0 mmol/L and −5.3 to 0.5 mmol/L respectively (Fig. S4C). Freshwater $SO_4^{2-}{}_{react}$ values range from −0.1 to 0.3 mmol/L.

DIC concentrations range from 3.7 to 5.7 mmol/L in fresh groundwaters, from 5.2 to 8.2 mmol/L in brackish samples and from 3.2 to 5.3 mmol/L in saline groundwaters. In fresh and brackish groundwaters the HCO_3^- concentration accounts for 83–94% of the DIC, while in saline groundwaters the HCO_3^- concentration accounts for 76–83% of the DIC. CO_2 accounts of the majority of the remaining carbonate speciation, accounting for 3–11% of DIC in fresh and brackish groundwaters and 3–6% of DIC in saline groundwaters. $\delta^{13}C_{DIC}$ values range from −11.0‰ to −5.8‰ in fresh groundwaters, from −11.4‰ to −2.3‰ in brackish groundwaters and from −9.4‰ to −2.2‰ in saline groundwaters (Fig. 4A, C). Seawater has a $\delta^{13}C_{DIC}$ value of 0.9‰. $^{14}C_{DIC}$ values range from 41.8 to 95.2 pmc in fresh groundwaters, from 8.7 to 97.2 pmc in brackish groundwaters and from 8.4 to 52.5 pmc in saline groundwaters (Fig. 4B, C). $^{14}C_{DIC}$ values decrease with increasing depth below ground surface ($r = 0.60$), while $\delta^{13}C_{DIC}$ values increase with increasing depth ($r = -0.56$). A very strong correlation between $^{14}C_{DIC}$ and $\delta^{13}C_{DIC}$ is also observed ($r = -0.94$; Fig. 4C).

^3H values range from 0.62 to 1.35 TU in fresh groundwaters, from 0.12 to 1.04 TU in brackish groundwaters and from 0.03 to 0.67 TU in saline groundwaters (Fig. 5A–C), suggesting that most groundwaters are modern and recharged within the past 50 years. A general trend is observed for all groundwater samples (except three wells: 11–90, 18–90 and 31–90), which shows decreasing $^{14}C_{DIC}$ values ($r = 0.76$) and $\delta^{13}C_{DIC}$ enrichment ($r = -0.64$) with decreasing ^3H concentration (Fig. 5A and B, respectively).

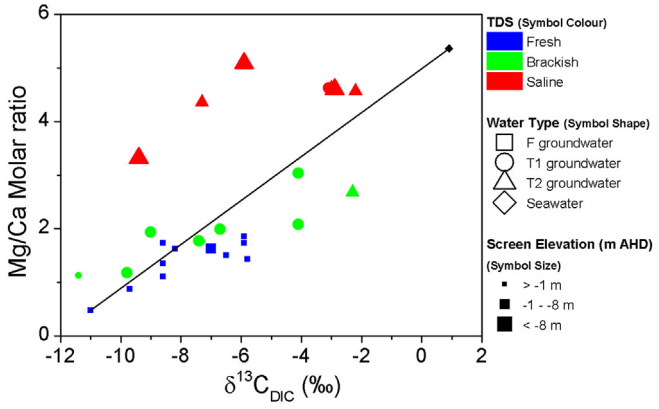

Fig. 3. Bivariate plot showing the molar ratio of Mg/Ca vs. $\delta^{13}C_{DIC}$ for groundwaters according to the TDS classification (Fresh: <1000 mg/L, Brackish: 1000–10,000 mg/L, Saline: 10,000–100,000 mg/L) outlined by Fetter (2001) and symbol size according to screen elevation. The figure also shows a conservative mixing line (solid line) between a freshwater and seawater end-member.

4.2. Organic chemistry

DOC concentrations range from 0.6 to 2.9 ppm in fresh groundwaters, 0.8 to 2.8 ppm in brackish samples and from 0.1 to 1.1 ppm in saline

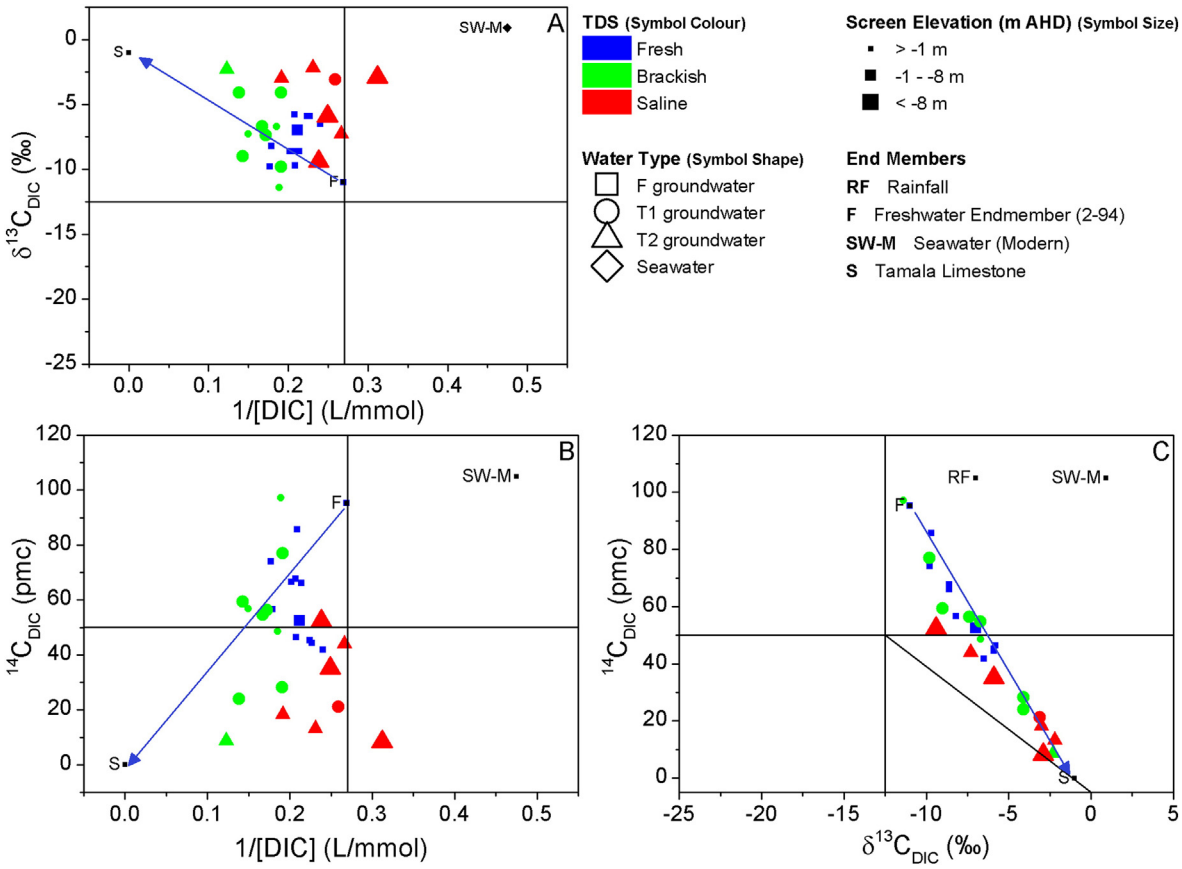

Fig. 4. Han and Plummer diagrams of $^{14}C_{DIC}$–$\delta^{13}C_{DIC}$–DIC diagrams (Han et al., 2012) of groundwater samples according to the TDS classification (Fresh: <1000 mg/L, Brackish: 1000–10,000 mg/L, Saline: 10,000–100,000 mg/L) outlined by Fetter (2001) and symbol size according to screen elevation. The blue arrows indicate evolution trajectories according to carbonate dissolution.

groundwaters. $\delta^{13}C_{DOC}$ values range from −26.6 to −24.7‰ in fresh groundwaters, from −28.6 to −24.7‰ in brackish groundwaters and from −31.1 to −23.9‰ in saline groundwaters. Deeper groundwaters tend to have less DOC compared to shallower groundwaters ($r = 0.30$), while $\delta^{13}C_{DOC}$ values throughout the system show little correlation with depth ($r = 0.10$). $^{14}C_{DOC}$ values range from 46.6 to 105.6 pMC across all groundwater samples, with saline samples showing the lowest $^{14}C_{DOC}$ values (46.6 to 67.0 pMC; Fig. 6). Freshwater $^{14}C_{DOC}$ values range from 88.9 to 105.6 pMC and brackish groundwaters range from 84.0 to 97.5 pMC. $^{14}C_{DOC}$ values decrease with increasing depth ($r = 0.55$) and decreasing ^{3}H ($r = 0.89$; Fig. 5C), while good correlation between $^{14}C_{DOC}$ and $^{14}C_{DIC}$ is also observed ($r = 0.71$; Fig. 6).

LC-OCD analysis shows that groundwater DOC is primarily composed of Humic Substances (as defined in Table S1), which constitute between 46 and 78% of the total DOC, while Building Blocks and LMW-neutral fractions constitute between 4 and 33% of the total DOC in most groundwaters (Fig. 7). The other fractions are omitted here due to their limited occurrence. Seawater contains 51% Humic Substances, 16% Building Blocks and 18% LMW-neutrals, with the remaining 14% of DOC composed of Biopolymers, LMW-acids and Hydrophobic organic carbon (HOC). Saline groundwaters with less ^{3}H and lower $^{14}C_{DOC}$ values tend to have higher proportions of Humic Substances compared to young fresh groundwaters (Fig. 7).

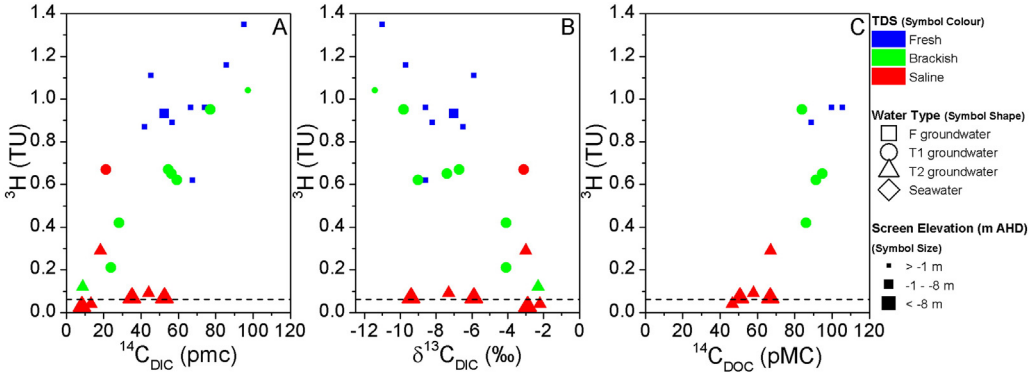

Fig. 5. Bivariate plots of ^{3}H vs. A) $^{14}C_{DIC}$, B) $\delta^{13}C_{DIC}$ and C) $^{14}C_{DOC}$ for groundwaters according to the TDS classification (Fresh: <1000 mg/L, Brackish: 1000–10,000 mg/L, Saline: 10,000–100,000 mg/L) outlined by Fetter (2001) and symbol size according to screen elevation. The dashed lines indicate the ^{3}H detection limit (0.06 TU).

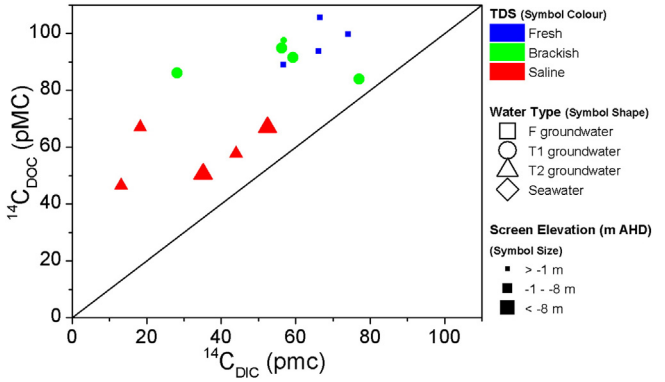

Fig. 6. Bivariate plot of $^{14}C_{DOC}$ vs. $^{14}C_{DIC}$ for groundwaters according to the TDS classification (Fresh: <1000 mg/L, Brackish: 1000–10,000 mg/L, Saline: 10,000–100,000 mg/L) outlined by Fetter (2001) and symbol size according to screen elevation. The black line indicates a 1:1 ratio.

5. Discussion

The following section discusses the geochemical evolution of waters from rainfall to fresh groundwater in the modern setting and then discusses the evolution of groundwaters in the transition zone of the aquifer to identify whether groundwaters of varying salinity have evolved under similar pathways to fresh waters and identify the occurrence of modern and old groundwaters in the transition zone. The data revealed three distinct water types (Fig. 8): fresh (F), Transition zone 1 (T1) and Transition zone 2 (T2) groundwaters, which evolved along alternate pathways described below.

5.1. Geochemical processes in the freshwater lens

The following section investigates the hydrochemical evolution in the Tamala Limestone on Rottnest Island between the surface and shallow groundwater, which encompasses the unsaturated zone and fresh groundwaters. The groundwaters are designated as F (Fresh) type waters, and occur at the top of the saturated zone. They are characterised by TDS values between 474 and 833 mg/L ($n = 12$), $^{14}C_{DIC}$ values between 41.8 and 95.2 pmc ($n = 12$), $^{14}C_{DOC}$ values between 88.9 and 105.6 pMC ($n = 4$) and ^{3}H values between 0.62 and 1.35 TU ($n = 9$). All waters located at the top of the water table (−1.0–0.1 m AHD) are evolved compared to rainfall, suggesting that the composition of F groundwater is largely governed by processes occurring in the unsaturated zone. These processes are explored by comparing the composition of rainwater with the freshest groundwater sample (well 2-94), which was determined according to its low TDS value (474 mg/L) and relatively low $\delta^{13}C_{DIC}$ value (−11.0‰), when compared to other groundwaters in the lens. The concentration of major dissolved ions in the rainwater are likely to increase prior to, and during infiltration due to a combination of evaporation and transpiration removing water but leaving behind the solutes. Seawater spray and salt dry deposition by aerosols onto the ground surface and vegetation in this coastal environment is also likely to be contributing to the enrichment of the infiltrating water (Appelo and Postma, 2005). As Cl^- is assumed to behave conservatively (in contrast to other solutes such as Ca and SO_4^{2-} which may participate in precipitation and dissolution reactions), it is used to determine the combined contribution from evapotranspiration and salt deposition. As such, average rainwater values for major cations and sulphate were adjusted by a concentration factor of 1.3 (Table 1), which was calculated by $[Cl\text{-}]_{well\ 2\text{-}94}/[Cl\text{-}]_{rainfall}$.

After rainfall infiltrates the soil, the limestone or carbonate minerals contained in the unsaturated zone are susceptible to dissolution reactions. This is due to dissolution of CO_2 produced in the soil, and the subsequent formation of carbonic acid:

$$CH_2O + O_2 \rightarrow CO_2 + H_2O \rightarrow H_2CO_3 \quad (5)$$

The carbonic acid in turn drives the dissolution of carbonate minerals and the release of Ca and HCO_3^- according to:

$$CaCO_3 + H_2CO_3 \leftrightarrow Ca^{2+} + 2HCO_3^- \quad (6)$$

P_{CO2} values range from $10^{-2.5}$ to $10^{-2.0}$ atm within the freshwater lens, which are one to two orders of magnitude higher than atmospheric partial pressure ($10^{-3.5}$ atm), and are indicative of CO_2 generation by root respiration and decay of labile organic material according to Eq. (5) (Hanson et al., 2000). Only small concentrations of DOC were observed within F groundwaters (average = 1.2 ppm; $n = 12$), which is likely due to biochemical processes such as oxidation to CO_2 gas and adsorption within the vadose zone, which can result in an 80% loss of DOC as it is transported downwards from the soil zone (Wassenaar et al., 1991a). The freshwater DOC is primarily composed of Humic Substances (48–64% of total DOC; $n = 12$; Fig. 7) and $\delta^{13}C_{DOC}$ signatures reflect a dominant C_3 organic matter source (−26.6‰ to −24.7‰; $n = 12$), suggesting that it originates from the decomposition of organic carbon in the soil zone. DO concentrations decline with increasing Cl^- concentration in the F groundwaters and range from 1.3–7.0 mg/L ($n = 12$; Fig. S3C), which is lower than concentrations due to equilibrium with the atmosphere. The low DO values, combined with high P_{CO2} values, support the hypothesis that organic matter is a source of CO_2 in the

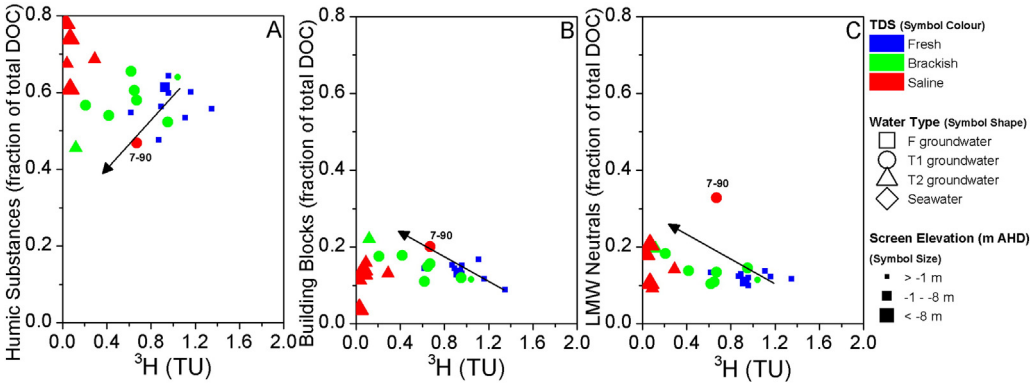

Fig. 7. Bivariate plots showing **A**) Humic Substances, **B**) Building Blocks and **C**) LMW-neutrals vs. ^{3}H. The results are expressed as fractions normalised to total DOC determined by LC-OCD analysis. Groundwaters are grouped according to the TDS classification (Fresh: <1000 mg/L, Brackish: 1000–10,000 mg/L, Saline: 10,000–100,000 mg/L) outlined by Fetter (2001) and symbol size according to screen elevation. Refer to Table S1 for a description of each DOC fraction. Arrows indicate the expected concentration trend of each DOC fraction over time if organic matter decomposition were occurring.

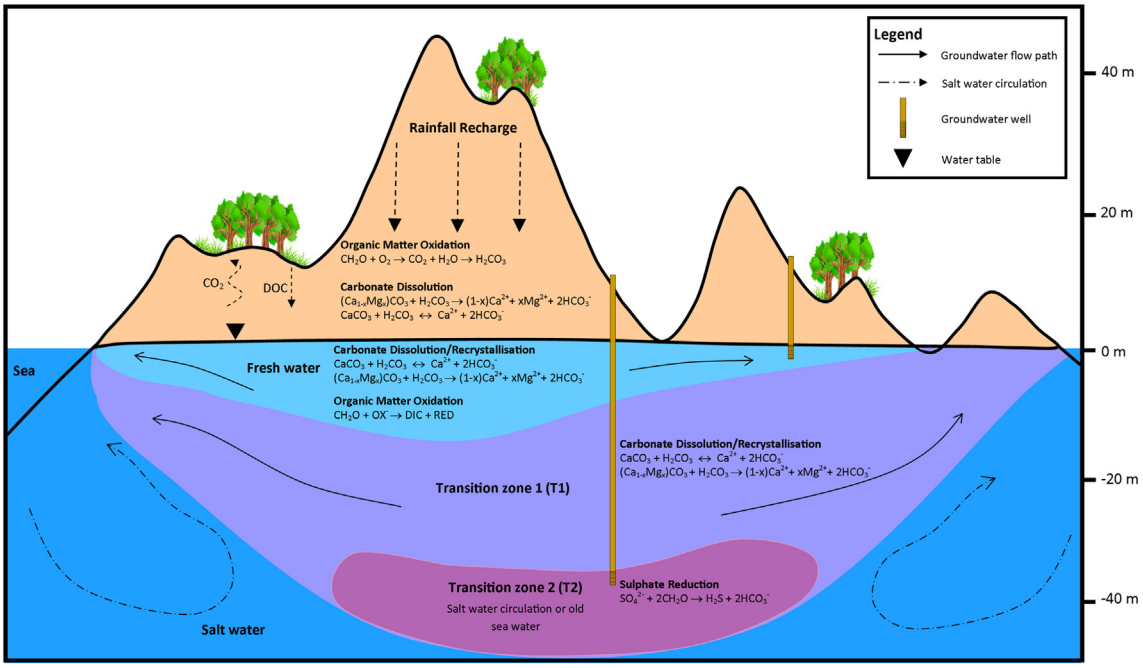

Fig. 8. A conceptual cross-section of the groundwater system on Rottnest Island, showing key processes and the three water types identified through this study: Fresh (F), Transition zone 1 (T1) and Transition zone 2 (T2). OX^- refers to a reactant undergoing oxidation while RED refers to a product that has been reduced.

unsaturated zone, and is oxidised by aerobic bacteria that consume available oxygen according to Eq. (5).

All groundwaters sampled at the top of the water table (−1.0 to 0.1 m AHD) are saturated with respect to calcite and aragonite (Table 1), which implies that infiltrating recharge waters react rapidly with carbonate minerals in the unsaturated zone and suggests that carbonate dissolution has occurred. As the Tamala limestone retains primary porosity, rapid fracture flow in the near surface is thought to be unlikely. As a result, relatively slow recharge would allow for carbonate dissolution to proceed to near completion in the shallow vadose zone, which can occur in hours to days (Svensson and Dreybrodt, 1992). The enriched $\delta^{13}C_{DIC}$ values also support the occurrence of carbonate dissolution, with values trending towards the $\delta^{13}C$ value of the Tamala Limestone (−1‰) determined by Meredith et al. (2012). This is also evidenced by the significant increase, by an order of magnitude, of Ca, Mg and HCO_3^- concentrations between (evapo-concentrated) rainfall and F groundwater at the top of the water table, as well as the [Ca + Mg]:HCO_3^- molar ratio (average 1:1.7; $n = 12$) that is close to the expected ratio (1:2) for Mg-calcite dissolution (Eq. (7); Fig. 2C). NETPATH modelling of recharge waters through the unsaturated zone predicts the dissolution of 1.2 mmol/kg H_2O of 30 mol% Mg-calcite (high Mg-calcite) and 0.4 mmol/kg H_2O of aragonite (Table S5) to form a fresh Ca, Mg-HCO_3^- dominated groundwater (2-94).

After the groundwater system becomes closed to soil CO_2, isotope exchange may occur as the groundwater DIC is exposed to solid carbonate in the aquifer via recrystallisation. Marine carbonate sediments, such as those found on Rottnest Island, generally consist of aragonite and high Mg-calcite [(Ca, Mg)CO_3] of biogenic origin (Appelo and Postma, 2005), which can undergo extensive recrystallisation when in contact with fresh water. Recrystallisation reactions involve the dissolution of less stable or slightly impure forms of calcium carbonate (e.g. aragonite and Sr or Mg substituted calcite) of marine or saline water origin and the precipitation of more stable forms (e.g. calcite) in fresh water (Kloppmann et al., 1998; Plummer and Sprinkle, 2001; Brown et al., 2014). The reactions are likely driven by small differences in Gibbs free energy of carbonates (Plummer and Sprinkle, 2001). The dissolution of Mg-calcite that results in the release of Mg can be represented by (Chapelle and Knobel, 1985):

$$(Ca_{1-x}Mg_x)CO_3 + H_2CO_3 \rightarrow (1-x)Ca^{2+} + xMg^{2+} + 2HCO_3^- \quad (7)$$

The incongruent dissolution of high Mg-calcite and the formation of more stable low Mg-calcite results in the release of Mg to the groundwater (Edmunds, 1980; Edmunds et al., 1987; Moore, 1989; Appelo and Postma, 2005; Stumm and Morgan, 2012) according to Eq. (7), which is observed on Rottnest Island through an excess of Mg in all F groundwaters ($Mg_{react} = 0.5$–1.1 mmol/L; $n = 12$). An increase in the Mg/Ca ratio with $\delta^{13}C_{DIC}$ enrichment (Moore, 1989) is also indicative of incongruent dissolution of high Mg-calcite (Fig. 3), with similar results observed in a study by Kloppmann et al. (1998). Aragonite will begin to be dissolved once the Mg-calcite is converted to calcite, thereby increasing the Sr/Ca ratio in the water (Moore, 1989). While a small increase in Sr was observed in all F groundwaters, the larger increase in Mg is likely caused by preferential loss of Mg from the high Mg-calcite as it undergoes dissolution and recrystallisation to pure calcite (Berner, 1967). The geochemical reactions between the freshest groundwater (well 2-94) and the most evolved F groundwater (well 3–77) was modelled using NETPATH and the results indicate that 4.5 mmol/kg H_2O of high Mg-calcite would dissolve while 3.5 mmol/kg H_2O of pure calcite would precipitate (Table S5), which further supports the occurrence of recrystallisation in the freshwater lens.

Carbonate dissolution should result in an increase in DIC as HCO_3^- is released according to Eqs. (6) and (7), and we would expect to see groundwaters increasing in both DIC and $\delta^{13}C$ along the blue arrow from end-member F towards end-member S in Fig. 4A. End-member F is the freshest groundwater just below the water table (well 2–94; $\delta^{13}C_{DIC} = -11$‰, DIC = 3.7 mmol/L, $^{14}C_{DIC} = 95.2$ pmc) and S is the carbonate mineral ($\delta^{13}C_S = -1$‰, $^{14}C_{DIC} = 0$ pMC). Only small increases in F groundwater DIC concentrations were observed (2.0 mmol/L; $n = 12$), which would result from the ~1.0 mmol/kg H_2O difference between the high Mg-calcite dissolved and calcite precipitated. During the recrystallisation dissolution/precipitation step,

carbon from the carbonate mineral is exchanged with groundwater DIC, with the concentration of DIC remaining relatively constant while $\delta^{13}C_{DIC}$ and $^{14}C_{DIC}$ values vary (Brown et al., 2014). Isotopic exchange between DIC and solid carbonate in F groundwater is supported by the Han and Plummer plots (Fig. 4A–C; Han et al., 2012), due to the variation in $\delta^{13}C_{DIC}$ values (−11.0 to −5.8‰; $n = 12$) without significant change in DIC concentration, and the strong correlation between increasing $\delta^{13}C_{DIC}$ and decreasing $^{14}C_{DIC}$ values (Fig. 4C). As recrystallisation lowers the ^{14}C activity of DIC, correction of this data would naturally be required if it is to be used to date the groundwater.

While carbonate dissolution and recrystallisation are the dominant geochemical reactions within the F groundwaters on Rottnest Island, other minor processes were also investigated. Ion exchange often plays an important role in determining the geochemistry of groundwater, especially in coastal areas where the mixing of fresh and saline groundwaters occurs (Andersen, 2001; Andersen et al., 2005; Appelo and Postma, 2005). The hydrochemical results show that all F groundwater samples have a slight depletion of Ca relative to conservative mixing, while over half of the F samples also have a slight depletion of Na. The occurrence of ionic exchange requires further investigation as the results do not show opposing trends of Ca depletion and Na enrichment that would generally be expected (Table S2). An excess of Mg is observed in all F groundwaters (Table S2), which is likely caused by the release of Mg during progressive recrystallisation of the carbonate minerals (Edmunds et al., 1987) rather than ion exchange. Iron and sulphate reduction reactions were also investigated, however they were not deduced to play a significant role in the F groundwaters. The presence of organic matter in the unsaturated zone however may influence the concentration of nitrate in the water. The observed NO_3^- concentration in F groundwaters (0.1–0.3 mmol/L; $n = 12$) may be caused by the oxidation of ammonia (not analysed) released from oxidising organic matter according to Eq. (8) (Appelo and Postma, 2005):

$$NH_4^+ + 2O_2 \rightarrow NO_3^- + H_2O + 2H^+ \quad (8)$$

Nitrogen in soil can occur in several forms including as organic nitrogen in plants through the fixation of atmospheric nitrogen and in bacteria associated with leguminoses, or in soil fauna (Canter, 1996). The transformation of organic nitrogen into NO_3^- leads to the production of H^+ (Eq. (8)), with the resulting drop in pH often being buffered by calcite dissolution in the soil and/or aquifer (Stadler et al., 2008). The nitrate formed in the unsaturated zone may then be leached into the groundwater and explain the excess NO_3^- in the F groundwaters. A related investigation at ANSTO that analysed nitrogen isotopes (^{15}N) of soils and groundwater on Rottnest Island determined a soil nitrogen source throughout the F groundwaters, which further supports the results found in this study (results not shown).

5.2. Groundwaters in the transition zone

Coastal aquifers are influenced by transition zone processes between fresh groundwater and seawater (Plummer, 1975; Andersen, 2001; Yechieli et al., 2001; Sivan et al., 2004; Andersen et al., 2005). These mixing processes, which can lead to an increase in salinity in an aquifer, have been previously investigated and determined to be a fundamental process governing groundwater hydrochemical and isotopic values on Rottnest Island (Bryan et al., 2016). The following section describes two groundwater types in the transition zone, which undergo carbonate mineral reactions described above, as well as additional reactions (Fig. 8).

The first transition zone groundwater type (T1) is characterised by TDS values ranging from 1040 to 20,676 mg/L ($n = 10$), $^{14}C_{DIC}$ values between 21.2 and 97.2 pmc ($n = 10$), $^{14}C_{DOC}$ between 84.0 and 97.5 pMC ($n = 4$) and ^{3}H values between 0.21 and 1.04 TU ($n = 9$). The lower $^{14}C_{DIC}$ values in these groundwaters imply either an older seawater source or water-rock interactions which dilutes and lowers the $^{14}C_{DIC}$ pool via carbonate dissolution and precipitation reactions, as discussed above. The presence of ^{3}H, combined with an increase in $\delta^{13}C_{DIC}$ values and a decrease in $^{14}C_{DIC}$ values (Fig. 4A–C), supports the occurrence of carbonate mineral processes, rather than an older source of seawater, to explain the $^{14}C_{DIC}$. The $^{14}C_{DOC}$ values are consistent with $^{14}C_{DOC}$ values observed in the young F groundwaters (Fig. 6). The DOC composition is also similar to that of F groundwaters, with comparable proportions of Humic Substances relative to total DOC (Fig. 7A), suggesting that it also originates primarily from the decomposition of organic carbon in the soil zone. One sample (well 7-90; Fig. 1), which was previously hypothesised to be undergoing the effects of modern seawater intrusion (Bryan et al., 2016), has a DOC composition similar to that of modern seawater (Fig. 7A–C). While further investigation is required, the DOC composition, combined with a modern ^{3}H signature and a high TDS value, further supports the hypothesis that modern seawater intrusion is occurring in the region around this well.

A continued increase in the Mg/Ca molar ratio compared to $\delta^{13}C_{DIC}$ values (Fig. 3), as well as an excess of Mg in most T1 groundwaters, suggests that recrystallisation may continue to occur. A small excess of both Ca and Na is observed in most of these waters which may be indicative of ionic exchange (Table S2; Fig. S4), however concurrent patterns of enrichment and depletion in these ions are not detected across samples, probably due to changes in Ca concentrations being rapidly buffered by carbonate precipitation and dissolution reactions. As such, temporal monitoring is required to definitely deduce the occurrence of ion exchange reactions.

The second group of groundwaters identified in the transition zone (T2) are those that have little to no measurable ^{3}H (0.03–0.29 TU; $n = 7$). These waters are characterised by higher TDS values (6868–29,675 mg/L; $n = 7$), $^{14}C_{DIC}$ values between 8.4 and 52.5 pmc ($n = 7$) and $^{14}C_{DOC}$ between 46.6 and 67.0 pMC ($n = 5$). A continued increase in $\delta^{13}C_{DIC}$ values and a decrease in $^{14}C_{DIC}$ values are observed throughout T2 groundwaters (Fig. 4A–C), which supports the occurrence of carbonate dissolution, however $^{14}C_{DOC}$ values are notably lower than all other groundwaters, ranging from 46.6 to 67.0 pMC. They are also characterised by a different DOC composition, with a higher proportion of Humic Substances relative to total DOC (Fig. 7A). Their DOC composition is also quite different from the DOC composition of modern seawater (Fig. 7A), which suggests these waters did not evolve along a similar pathway to modern day waters of the freshwater lens or from modern seawater intrusion. This will be discussed in further detail below.

An excess of Mg was observed in some of the T2 groundwaters, however the Mg/Ca molar ratio appears to follow a different trajectory to the F and T1 groundwaters (Fig. 3). This is likely the result of further mixing with seawater, which has a significantly higher Mg concentration. As for T1 groundwaters, concurrent patterns of cation enrichment and deficit were not detected across the T2 samples. The most saline groundwaters have a significant Na deficit ($Na_{react} = -44.6$ to −22.7 mmol/L; $n = 3$), however this is not countered by an excess in other cations that would suggest concurrent patterns of ion exchange.

The degradation of organic matter (CH_2O) via various redox reactions was also investigated, as they can affect the dissolved carbonate composition, change endmember compositions prior to mixing, and influence the carbonate mineral saturation states of mixed groundwaters (Stoessell et al., 1993; Whitaker and Smart, 1997; Andersen, 2001). Since low NO_3^- concentrations were observed throughout the aerobic part of the profile (0.1–0.7 mmol/L) and since additional amounts of NO_3^- released from degradation of organic matter is approximately limited by the Redfield ratio of organic matter (0.15 mol of N released per mol of C oxidised), the amount of denitrification in the mixing zone is assessed to be less than ~1 mmol/L of DIC released according to the reaction equation for denitrification:

$$5CH_2O + 4NO_3^- \rightarrow 2N_2 + H^+ + 5HCO_3^- + 2H_2O \quad (9)$$

An absence of dissolved iron throughout the mixing profile suggests that iron-oxide reduction does not play a major role, although Fe^{2+}

released from iron-oxide reduction may be masked by reaction with H_2S for sulfidogenic conditions to form insoluble FeS or FeS_2 solids. A deficit of sulphate in the more saline T1 and T2 groundwaters was determined, which is commonly observed when seawater with a high sulphate content intrudes into an anoxic costal aquifer (Nadler et al., 1980; Hahn, 1991; Stuyfzand, 1993; Barker et al., 1998; Logan et al., 1999; Andersen, 2001; Yamanaka and Kumagai, 2006). In most cases it can be attributed to SO_4^{2-} reduction according to:

$$SO_4^{2-} + 2CH_2O \rightarrow H_2S + 2HCO_3^- \quad (10)$$

In some cases however, SO_4^{2-} depletion by gypsum precipitation in the transition zone has been modelled (Gomis-Yagües et al., 2000). Together with SO_4^{2-} depletion, gypsum precipitation leads to Ca depletion according to:

$$SO_4^{2-} + Ca^{2+} \rightarrow CaSO_4 \quad (11)$$

This reaction could therefore trigger renewed carbonate mineral dissolution. However, gypsum is subsaturated in all mixing groundwaters (SI_{gypsum} average $= -1.37$ mg/L; $n = 17$) and hence unlikely to precipitate. Elevated DO concentrations in most T1 groundwaters (average $=$ 1.6 mg/L; $n = 10$) would inhibit sulphate reduction, however sulphate reduction was hypothesised to occur in the more saline T2 groundwaters, due to low DO values (0.1–0.9 mg/L; $n = 7$; Fig. S3C), a deficit of SO_4^{2-} ($SO_4^{2-}{}_{react} = -5.3$–$0.5$ mmol/L; $n = 7$) and an excess of HCO_3^- ($HCO_{3react} = 0.4$–3.8 mmol/L; $n = 7$; Fig. S4C). While the SO_4^{2-} depletion is more pronounced than the HCO_3^- enrichment in some of the T2 groundwaters, it is possible that excess HCO_3^- could be removed through carbonate precipitation reactions, which can explain the difference between the expected concentrations.

5.3. Old seawater in the transition zone

As discussed above, the lower $^{14}C_{DOC}$ values (<68 pMC) and the different DOC composition of the T2 groundwaters indicate distinct groundwaters. The spatial distribution of the $^{14}C_{DOC}$ values show that lower values are associated with areas of the lens that have receded since the 1970's (Fig. S6). This suggests that as the volume of fresh water is reduced due to climate change and groundwater abstraction and a subsequent thinning of the lens occurs (Bryan et al., 2016), saline ^{3}H-free groundwaters in the transition zone can rise to a point where they become evident within the wells sampled.

Compared to F and T1 groundwaters, T2 waters are characterised by more Humic Substances and less Building Blocks relative to total DOC (Fig. 7A,B). The continued occurrence of a high proportion of Humic Substances in deeper, saline groundwaters is the opposite of what is expected. Humic Substances, which are a mixture of acids containing carboxyl and phenolate groups produced by the biodegradation of dead organic matter (molecular weight ~1000 Da), can be of terrestrial or marine origin. They are generally expected to be easily sorbed and broken down to lower weight molecules (such as Building Blocks or LMW-neutrals; refer to process arrows in Fig. 7) via a number of physical, chemical, and biological processes in the subsurface, such as biodegradation. These processes can have a significant effect on both the concentration and composition of DOC (Thurman, 1985b; Schiff et al., 1990; Schiff et al., 1997; Sun et al., 1997; Tye and Lapworth, 2016). As a high proportion of Humic Substances remain in the deeper saline waters and the $^{14}C_{DOC}$ values are considerably lower than all other groundwaters, it is suggested that the DOC originated from another source compared to that of F and T1 groundwaters.

One potential source of groundwater DOC may be solid phase organic carbon originating from the aquifer matrix (Thurman, 1985b), with DOC arising from in-situ abiotic or bacterial decomposition of buried peat, paleosols, organic rich horizons, or from the polymerisation of low molecular weight organic compounds (Krom and Sholkovitz, 1977; Wassenaar et al., 1991a). The DOC may be attributed to paleosols which have been identified in the unsaturated zone of the Tamala Limestone (Playford and Leech, 1977; Brooke et al., 2014; Lipar and Webb, 2014; Lipar and Webb, 2015), which could contribute old organic matter to the groundwater during recharge. However, the groundwater flow path for samples with high salinity (>50% seawater) would generally be from the ocean rather than from the land surface, which would limit the influence of these paleosols on the groundwater DOC concentration and composition. Additionally, as a result of the timing of paleosol deposition in the unsaturated zone (>70 ka), we would expect significantly lower $^{14}C_{DOC}$ values if the groundwater DOC composition was heavily influenced by paleosols.

Alternatively, we propose that these ^{3}H–free groundwaters are older groundwaters resulting from either the slow circulation of water within the subsurface seawater wedge, or from seawater intrusion caused by a past sea level highstand. The slow circulation of water within the seawater wedge has been shown to result in distinctly higher ages in the transition zone compared to those in the underlying saltwater or overlying freshwater (Post et al., 2013). The saline groundwaters also could result from trapped remnant seawater remaining after sea level highstands associated with glacial/interglacial cycles in the late Pleistocene and early Holocene, with other studies documenting such waters as a result of seawater intrusion due to sea level rise (De Breuck and De Moor, 1991; Hahn, 1991; Bear et al., 1999; Yechieli et al., 2009). However, the permeable nature of the Tamala limestone would likely lead to relatively fast re-equilibration of the saltwater-freshwater interface after sea level highstands (occurring ~3–7 ka ago) well before present, making this alternative less likely.

While the saline, ^{3}H-free water $^{14}C_{DOC}$ values on their own provide a rough residence time estimation of between 3 and 7 ka (using an initial ^{14}C activity value (A_0) of 100 pMC), which coincides with the aforementioned sea level high-stand, caution should be observed. Before $^{14}C_{DOC}$ can be used as a reliable tracer of residence time, further investigation into the various carbon sources, their age, the impact of fractionation and dilution by ^{14}C-depleted organic carbon on the final $^{14}C_{DOC}$ value and the retardation of DOC in the aquifer matrix are required. While additional investigations are required to accurately identify organic carbon processes of the ^{3}H–free, saline T2 groundwaters and apply $^{14}C_{DOC}$ as a dating method, this study has shown how combining isotopic techniques (stable and radioactive tracers) with the characterisation of the DOC identified the occurrence of an old saltwater source and has shown that these groundwaters did not evolve along a similar pathway to the modern day waters of the freshwater lens.

6. Conclusions

This study aimed to investigate both the inorganic and organic facets of the carbon cycle in groundwaters throughout a freshwater lens and transition zone of an island aquifer and identify the carbon sources that contribute to the groundwater system. We traced the geochemical evolution of waters from rainfall to fresh groundwater and it was determined to be dominated by carbonate mineral recrystallisation reactions, with the dissolution of high Mg-calcite and the precipitation of calcite quantified. This was done to then assess whether other groundwaters of varying salinity had evolved under similar pathways. The ^{3}H values in T1 groundwaters indicate that, like fresh groundwaters, these waters are mostly modern. Saline, ^{3}H-free T2 groundwaters underlying the freshwater lens were shown to be older and did not evolve along a similar pathway to modern day waters of the freshwater lens. As such, the T2 groundwaters are suggested to result from either the slow circulation of water within the seawater wedge, which has been shown to result in distinctly higher ages in the transition zone, or from old remnant sea water resulting from past sea level highstands. While further investigations are required to identify the origin of the T2 groundwaters, this study has identified their occurrence and shown that they did not evolve along a similar pathway to the modern waters of the freshwater lens. This study has also shown that a combined approach using ^{14}C and

^{13}C carbon isotope values for both DIC and DOC and the composition of DOC, as well as hydrochemical and ^{3}H measurements, can provide invaluable information regarding the transformation of carbon in a groundwater system, the evolution of fresh groundwater recharge and the occurrence of older waters that evolved along a different pathway. This is important for understanding the evolution of groundwaters and for residence time calculations, as well as for the long term management of the freshwater lens on Rottnest Island, as well as on other islands globally.

Acknowledgements

The authors wish to thank the Rottnest Island Authority (RIA), especially Cassyanna Thomas, Luke Wheat and Shane Kearney for their ongoing support of this project. The authors would also like to thank Suzanne Hollins, Head of Research at the Australian Nuclear Science and Technology Organisation (ANSTO) for her ongoing support as well as various ANSTO personnel including Robert Chisari, Kellie-Anne Farrawell, Barbora Gallagher, Scott Allchin, Henri Wong and Chris Vardanega for their assistance in chemical and isotopic analysis, Geraldine Jacobsen, Alan Williams, Fiona Bertuch, Simon Varley and Riley Van De Voorde, for their assistance in radiocarbon dating and Chris Dimovski and Stuart Hankin for their assistance with field trip preparation. Thanks go to Khorshed Chinu from the Mark Wainwright Analytical Centre at UNSW for her assistance with LC-OCD analysis. We also thank four anonymous peer reviewers for their comments which helped to improve the manuscript, and the editor of Science of the Total Environment. Finally, thanks to G Wells, E Wells, M Bryan and A Rae for their assistance with proof reading.

Appendix A. Supplementary data

Supplementary data to this article can be found online at http://dx.doi.org/10.1016/j.scitotenv.2017.06.094.

References

Andersen, M.S., 2001. Geochemical Processes at a Seawater-Freshwater Interface. Technical University of Denmark, Kgs. Lyngby (PhD Thesis).
Andersen, M.S., Nyvang, V., Jakobsen, R., Postma, D., 2005. Geochemical processes and solute transport at the seawater/freshwater interface of a sandy aquifer. Geochim. Cosmochim. Acta 69 (16), 3979–3994.
Appelo, C.A.J., Postma, D., 2005. Geochemistry, Groundwater and Pollution. Rotterdam, A.A. Balkema.
Aravena, R., Wassenaar, L.I., Plummer, L.N., 1995. Estimating 14C groundwater ages in a methanogenic aquifer. Water Resour. Res. 31 (9), 2307–2317.
Barker, A.P., Newton, R.J., Bottrell, S.H., Tellam, J., 1998. Processes affecting groundwater chemistry in a zone of saline intrusion into an urban sandstone aquifer. Appl. Geochem. 13 (6), 735–749.
Bastian, L., 1996. Residual soil mineralogy and dune subdivision, swan coastal plain, Western Australia. Aust. J. Earth Sci. 43 (1), 31–44.
Bear, J., Cheng, A.H.-D., Sorek, S., Ouazar, D., Herrera, I., 1999. Seawater Intrusion in Coastal Aquifers: Concepts, Methods and Practices. Springer Science & Business Media.
Berner, R.A., 1967. Comparative dissolution characteristics of carbonate minerals in the presence and absence of aqueous magnesium ion. Am. J. Sci. 265 (1), 45–70.
BOM, 2016. Australian Government Bureau of Meteorology - Climate Averages Tables, Rottnest Island. Retrieved 22/02/2016, from. http://www.bom.gov.au/climate/averages/tables/cw_009193.shtml.
Brooke, B., 2001. The distribution of carbonate eolianite. Earth Sci. Rev. 55 (1), 135–164.
Brooke, B., Olley, J., Pietsch, T., Playford, P., Haines, P., Murray-Wallace, C., Woodroffe, C., 2014. Chronology of Quaternary coastal aeolianite deposition and the drowned shorelines of southwestern Western Australia–a reappraisal. Quat. Sci. Rev. 93, 106–124.
Brown, S., Nicholls, R.J., Hanson, S., Brundrit, G., Dearing, J.A., Dickson, M.E., Gallop, S.L., Gao, S., Haigh, I.D., Hinkel, J., 2014. Shifting perspectives on coastal impacts and adaptation. Nat. Clim. Chang. 4 (9), 752–755.
Bryan, E., Meredith, K.T., Baker, A., Post, V.E.A., Andersen, M.S., 2016. Island groundwater resources, impacts of abstraction and a drying climate: Rottnest Island, Western Australia. J. Hydrol. 542, 704–718.
Canter, L.W., 1996. Nitrates in groundwater. CRC press, Boca Raton, Florida.
Cartwright, I., Fifield, L.K., Morgenstern, U., 2013. Using 3 H and 14 C to constrain the degree of closed-system dissolution of calcite in groundwater. Appl. Geochem. 32, 118–128.
Chapelle, F.H., Knobel, L.L., 1985. Stable carbon isotopes of HCO3 in the Aquia aquifer, Maryland: evidence for an isotopically heavy source of CO2. Ground Water 23 (5), 592–599.
Clark, I., Fritz, P., 1997. Environmental Isotopes in Hydrology. Lewis Publishers.
Coshell, L., Rosen, M.R., 1994. Stratigraphy and Holocene history of Lake Hayward, Swan coastal plain wetlands, western Australia. SEPM Spec. Publ. 50, 173–188.
Craig, H., 1953. The geochemistry of the stable carbon isotopes. Geochim. Cosmochim. Acta 3 (2–3), 53–92.
De Breuck, W., De Moor, G., 1991. The evaluation of coastal aquifer of Belgium. Hydrogeology of Salt Water Intrusion: A Selection of SWIM papers. vol. 2. IWMI, Battaramulla, Sri Lanka, pp. 35–48.
Edmunds, W., 1980. The hydrogeochemical characteristics groundwaters in the Sirte Basin, using strontium and other elements. The Geology of Libya 2, 703–714.
Edmunds, W., 2009. Geochemistry's vital contribution to solving water resource problems. Appl. Geochem. 24 (6), 1058–1073.
Edmunds, W., Cook, J., Darling, W., Kinniburgh, D., Miles, D., Bath, A., Morgan-Jones, M., Andrews, J., 1987. Baseline geochemical conditions in the chalk aquifer, Berkshire, UK: a basis for groundwater quality management. Appl. Geochem. 2 (3), 251–274.
Edward, D., 1983. Inland waters of Rottnest Island. J. R. Soc. West. Aust. 66, 41–47.
Edward, D., Watson, J., 1959. Fresh water and brackish water swamps of Rottnest Island. J. R. Soc. West. Aust. 42, 85–86.
Fairbridge, R.W., Teichert, C., 1953. Soil horizons and marine bands in the coastal limestones of Western Australia. J. Proc. R. Soc. NSW 86, 68–87.
Fan, Y., 2016. Groundwater: how much and how old? Nat. Geosci. 9 (2), 93–94.
Fetter, C.W., 2001. Applied Hydrogeology. Macmillan College Publishing Inc, New York.
Fink, D., Hotchkis, M., Hua, Q., Jacobsen, G., Smith, A., Zoppi, U., Child, D., Mifsud, C., van der Gaast, H., Williams, A., 2004. The ANTARES AMS facility at ANSTO. Nucl. Instrum. Methods Phys. Res., Sect. B 223, 109–115.
Gomis-Yagües, V., Boluda-Botella, N., Ruiz-Beviá, F., 2000. Gypsum precipitation/dissolution as an explanation of the decrease of sulphate concentration during seawater intrusion. J. Hydrol. 228 (1), 48–55.
Gouramanis, C., Dodson, J., Wilkins, D., De Deckker, P., Chase, B., 2012. Holocene palaeoclimate and sea level fluctuation recorded from the coastal Barker Swamp, Rottnest Island, south-western Western Australia. Quat. Sci. Rev. 54, 40–57.
Gozzard, J.R., 2007. Geology and landforms of the Perth region. Geological Survey of Western Australia 126.
Gozzard, J.R., 2011. WA coast: Rottnest Island. Geological Survey of Western Australia digital data product.
Gröning, M., Lutz, H., Roller-Lutz, Z., Kralik, M., Gourcy, L., Pöltenstein, L., 2012. A simple rain collector preventing water re-evaporation dedicated for δ18O and δ2H analysis of cumulative precipitation samples. J. Hydrol. 448, 195–200.
Hahn, J., 1991. Aspects of groundwater salinization in the Wittmund (East Friesland) coastal area. Hydrogeology of Salt Water Intrusion—a Selection of SWIM Papers. II, pp. 251–270.
Han, L.-F., Plummer, L.N., Aggarwal, P., 2012. A graphical method to evaluate predominant geochemical processes occurring in groundwater systems for radiocarbon dating. Chem. Geol. 318, 88–112.
Hanson, P., Edwards, N., Garten, C., Andrews, J., 2000. Separating root and soil microbial contributions to soil respiration: a review of methods and observations. Biogeochemistry 48 (1), 115–146.
Hearty, P.J., 2003. Stratigraphy and timing of eolianite deposition on Rottnest Island, Western Australia. Quat. Res. 60 (2), 211–222.
Hearty, P.J., O'Leary, M.J., 2008. Carbonate eolianites, quartz sands, and Quaternary sea-level cycles, Western Australia: a chronostratigraphic approach. Quat. Geochronol. 3 (1), 26–55.
Huber, S.A., Balz, A., Abert, M., Pronk, W., 2011. Characterisation of aquatic humic and non-humic matter with size-exclusion chromatography–organic carbon detection–organic nitrogen detection (LC-OCD-OND). Water Res. 45 (2), 879–885.
Ingerson, E., Pearson, F., 1964. Estimation of age and Rate of Motion of Groundwater by the ^{14}C Method. Maruzen, Tokyo.
Kalin, R.M., 2000. Radiocarbon dating of groundwater systems. In: Cook, P., Herczeg, A. (Eds.), Environmental Tracers in Subsurface Hydrology. Kluwer, New York, pp. 111–144.
Kendrick, G.W., Wyrwoll, K.-H., Szabo, B.J., 1991. Pliocene-Pleistocene coastal events and history along the western margin of Australia. Quat. Sci. Rev. 10 (5), 419–439.
Kloppmann, W., Dever, L., Edmunds, W., 1998. Residence time of chalk groundwaters in the Paris Basin and the North German Basin: a geochemical approach. Appl. Geochem. 13 (5), 593–606.
Krom, M., Sholkovitz, E., 1977. Nature and reactions of dissolved organic matter in the interstitial waters of marine sediments. Geochim. Cosmochim. Acta 41 (11), 1565–1574.
Lipar, M., Webb, J., 2014. Middle–late Pleistocene and Holocene chronostratigraphy and climate history of the Tamala Limestone, Cooloongup and Safety Bay Sands, Nambung National Park, southwestern Western Australia. Aust. J. Earth Sci. 61 (8), 1023–1039.
Lipar, M., Webb, J.A., 2015. The formation of the pinnacle karst in Pleistocene aeolian calcarenites (Tamala Limestone) in southwestern Australia. Earth Sci. Rev. 140, 182–202.
Logan, W.S., Auge, M.P., Panarello, H.O., 1999. Bicarbonate, sulfate, and chloride water in a shallow, clastic-dominated coastal flow system, Argentina. Groundwater 37 (2), 287–295.
Mauz, B., Hijma, M., Amorosi, A., Porat, N., Galili, E., Bloemendal, J., 2013. Aeolian beach ridges and their significance for climate and sea level: concept and insight from the Levant coast (East Mediterranean). Earth Sci. Rev. 121, 31–54.
Meredith, K., Cendón, D.I., Pigois, J.-P., Hollins, S., Jacobsen, G., 2012. Using 14C and 3H to delineate a recharge 'window' into the Perth Basin aquifers, North Gnangara groundwater system, Western Australia. Sci. Total Environ. 414, 456–469.

Meredith, K., Han, L., Hollins, S., Cendón, D., Jacobsen, G., Baker, A., 2016. Evolution of chemical and isotopic composition of inorganic carbon in a complex semi-arid zone environment: consequences for groundwater dating using radiocarbon. Geochim. Cosmochim. Acta 188, 352–367.
Mook, W., 1980. Carbon-14 in hydrogeological studies. In: F., P., F., J.Ch. (Eds.), Handbook of Environmental Isotope Geochemistry. Elsevier, Amsterdam, pp. 49–74.
Mook, W.G., Van Der Plicht, J., 1999. Reporting ^{14}C activities and concentrations. Radiocarbon 41 (3), 227–239.
Moore, C.H., 1989. Meteoric diagenetic environments, chapter 7. Dev. Sedimentol. 46, 177–217.
Mory, A.J., 1995. Geology of the Wedge Island 1:100.000 sheet. Perth. Geological Survey of Western Australia 19.
Mucci, A., 1987. Influence of temperature on the composition of Magnesian calcite overgrowths precipitated from seawater. Geochim. Cosmochim. Acta 51 (7), 1977–1984.
Munnich, K., 1957. Messung des 14C-Gehalts von hartem Grundwasser. Naturwissenschaften 44, 32–39.
Murphy, E.M., Davis, S.N., Long, A., Donahue, D., Jull, A., 1989a. Characterization and isotopic composition of organic and inorganic carbon in the milk river aquifer. Water Resour. Res. 25 (8), 1893–1905.
Murphy, E.M., Davis, S.N., Long, A., Donahue, D., Jull, A.J.T., 1989b. ^{14}C in fractions of dissolved organic carbon in ground water. Nature 337 (6203), 153–155.
Nadler, A., Magaritz, M., Mazor, E., 1980. Chemical reactions of sea water with rocks and freshwater: experimental and field observations on brackish waters in Israel. Geochim. Cosmochim. Acta 44 (6), 879–886.
Parkhurst, D., Appelo, C., 2013. Description of input and examples for PHREEQC version 3-A computer program for speciation, batch-reaction, one-dimensional transport, and inverse geochemical calculations. U.S. Geological Survey Techniques and Methods. Book 6 chap. A43, 497 p.
Pearson, F., Hanshaw, B., 1970. Sources of dissolved carbonate species in groundwater and their effects on carbon-14 dating. Isotope Hydrology 271–286.
Pearson, F., White, D., 1967. Carbon 14 ages and flow rates of water in Carrizo Sand, Atascosa County, Texas. Water Resour. Res. 3 (1), 251–261.
Pedoja, K., Husson, L., Johnson, M.E., Melnick, D., Witt, C., Pochat, S., Nexer, M., Delcaillau, B., Pinegina, T., Poprawski, Y., 2014. Coastal staircase sequences reflecting sea-level oscillations and tectonic uplift during the Quaternary and Neogene. Earth Sci. Rev. 132, 13–38.
Pettersson, C., Arsenie, I., Ephraim, J., Boren, H., Allard, B., 1989. Properties of fulvic acids from deep groundwaters. Sci. Total Environ. 81, 287–296.
Playford, P.E., 1997. Geology and hydrogeology of Rottnest Island, Western Australia. In: Vacher, H.L., Quinn, T. (Eds.), Geology and Hydrogeology of Carbonate Islands. 54. Elsevier Science, pp. 783–810.
Playford, P.E., Cockbain, A.E., Berry, P., Roberts, A.P., Haines, P.W., Brooke, B., 2013. The geology of Shark Bay. Geological Survey of Western Australia, Bulletin 146 281p.
Playford, P.E., Leech, R.E.J., 1977. Geology and hydrology of Rottnest Island. Geological Survey of Western Australia Report 6.
Playford, P.E., Low, G.H., Cockbain, A.E., 1976. Geology of the Perth Basin, Western Australia, geological Survey of Western Australia. Bulletin 124.
Plummer, L., 1975. Mixing of sea water with calcium carbonate ground water. Geol. Soc. Am. Mem. 142, 219–236.
Plummer, L., Prestemon, E., Parkhurst, D., 1991. An interactive code (NETPATH) for modeling net geochemical reactions along a flow path Version 2.0. US Geological Survey Water-Resources Investigations Report. Reston, Virginia. 231.
Plummer, L.N., Glynn, P.D., 2013. Radiocarbon dating in groundwater systems. Isotope Methods for Dating Old Groundwaters. Chapter 4. International Atomic Energy Agency (IAEA), Vienna, pp. 33–89.
Plummer, N.L., Sprinkle, C.L., 2001. Radiocarbon dating of dissolved inorganic carbon in groundwater from confined parts of the Upper Floridan aquifer, Florida, USA. Hydrogeol. J. 9 (2), 127–150.
Post, V.E., Vandenbohede, A., Werner, A.D., Teubner, M.D., 2013. Groundwater ages in coastal aquifers. Adv. Water Resour. 57, 1–11.
Price, D.M., Brooke, B.P., Woodroffe, D., C., 2001. Thermoluminescence dating of aceolianites from Lord Howe Island and South-West Western Australian. Quat. Sci. Rev. 20 (5), 841–846.
Purdy, C., Burr, G., Rubin, M., Helz, G., Mignerey, A., 1992. Dissolved organic and inorganic C-14 concentrations and ages for coastal-plain aquifers in southern Maryland. Radiocarbon 34 (3), 654–663.
Rippey, M., Hobbs, R., 2003. The effects of fire and quokkas (*Setonix brachyurus*) on the vegetation of Rottnest Island, Western Australia. J. R. Soc. West. Aust. 86 (2), 49–60.
Rowe, M., Bristow, C., 2015. Sea-level controls on carbonate beaches and coastal dunes (eolianite): lessons from Pleistocene Bermuda. Geol. Soc. Am. Bull. 127 (11−12), 1645–1665.
Rutlidge, H., Andersen, M.S., Baker, A., Chinu, K.J., Cuthbert, M.O., Jex, C.N., Marjo, C.E., Markowska, M., Rau, G.C., 2015. Organic characterisation of cave drip water by LC-OCD and fluorescence analysis. Geochim. Cosmochim. Acta 166, 15–28.
Schiff, S., Aravena, R., Trumbore, S., Hinton, M., Elgood, R., Dillon, P., 1997. Export of DOC from forested catchments on the Precambrian Shield of Central Ontario: clues from 13C and 14C. Biogeochemistry 36 (1), 43–65.
Schiff, S., Aravena, R., Trumbore, S.E., Dillon, P., 1990. Dissolved organic carbon cycling in forested watersheds: a carbon isotope approach. Water Resour. Res. 26 (12), 2949–2957.
Sivan, O., Yechieli, Y., Herut, B., Lazar, B., 2004. Geochemical evolution and timescale of seawater intrusion into the coastal aquifer of Israel. Geochim. Cosmochim. Acta 69 (3), 579–592.
Smith, R.A., 1985. Effect of pumping on "freshwater" seeps, Rottnest Island. Hydrogeology Report 2623. 16. Western Australia Geological Survey, Perth.
Spiker, E., Rubin, M., 1975. Petroleum pollutants in surface and groundwater as indicated by the carbon-14 activity of dissolved organic carbon. Science 187 (4171), 61–64.
Stadler, S., Osenbrück, K., Knöller, K., Suckow, A., Sültenfuß, J., Oster, H., Himmelsbach, T., Hötzl, H., 2008. Understanding the origin and fate of nitrate in groundwater of semi-arid environments. J. Arid Environ. 72 (10), 1830–1842.
Stoessell, R.K., Moore, Y.H., Coke, J.G., 1993. The occurrence and effect of sulfate reduction and sulfide oxidation on coastal limestone dissolution in Yucatan cenotes. Ground Water 31 (4), 566–575.
Stumm, W., Morgan, J.J., 2012. Aquatic Chemistry: Chemical Equilibria and Rates in Natural Waters. John Wiley & Sons.
Stuyfzand, P.J., 1993. Hydrochemistry and Hydrology of the Coastal Dune Area of the Western Netherlands. Vrije Universiteit Amsterdam.
Sun, L., Perdue, E., Meyer, J., Weis, J., 1997. Use of elemental composition to predict bioavailability of dissolved organic matter in a Georgia river. Limnol. Oceanogr. 42 (4), 714–721.
Svensson, U., Dreybrodt, W., 1992. Dissolution kinetics of natural calcite minerals in CO2-water systems approaching calcite equilibrium. Chem. Geol. 100 (1–2), 129–145.
Swezey, C.S., Fitzwater, B.A., Whittecar, G.R., Mahan, S.A., Garrity, C.P., González, W.B.A., Dobbs, K.M., 2016. The Carolina Sandhills: Quaternary eolian sand sheets and dunes along the up dip margin of the Atlantic Coastal Plain province, southeastern United States. Quat. Res. 86 (3), 271–286.
Thurman, E.M., 1985a. Humic substances in groundwater. In: Aiken, G.R., McKnight, D.M., Wershaw, R.L., MacCarthy, P. (Eds.), Humic Substances in Soil, Sediment, and Water: Geochemistry, Isolation and Characterization. John Wiley & Sons.
Thurman, E.M., 1985b. Organic Geochemistry of Natural Waters. Springer, Netherlands.
Tye, A., Lapworth, D., 2016. Characterising changes in fluorescence properties of dissolved organic matter and links to N cycling in agricultural floodplains. Agric. Ecosyst. Environ. 221, 245–257.
Vacher, H.L., 1997. Introduction: varieties of carbonate islands and a historical perspective. In: Vacher, H.L., Quinn, T.M. (Eds.), Geology and Hydrogeology of Carbonate Islands. Elsevier, Amsterdam, pp. 1–33.
Vacher, H.L., Quinn, T.M., 2004. Geology and hydrogeology of carbonate Islands. Dev. Sedimentol. 54, 948.
Van Veen, J., Paul, E.A., 1978. The use of tracers to determine the dynamic nature of organic matter. 11th International Congress of Soil Science. Edmonton, Canada.
Wassenaar, L., Aravena, R., Fritz, P., Barker, J., 1990a. Isotopic composition (^{13}C, ^{14}C, ^{2}H) and geochemistry of aquatic humic substances from groundwater. Org. Geochem. 15 (4), 383–396.
Wassenaar, L., Aravena, R., Fritz, P., Barker, J., 1991a. Controls on the transport and carbon isotopic composition of dissolved organic carbon in a shallow groundwater system, Central Ontario, Canada. Chem. Geol. Isot. Geosci. 87 (1), 39–57.
Wassenaar, L., Aravena, R., Hendry, J., Fritz, P., 1991b. Radiocarbon in dissolved organic carbon, a possible groundwater dating method: case studies from western Canada. Water Resour. Res. 27 (8), 1975–1986.
Wassenaar, L., Hendry, M., Aravena, R., Fritz, P., 1990b. Organic carbon isotope geochemistry of clayey deposits and their associated porewaters, southern Alberta. J. Hydrol. 120 (1–4), 251–270.
Wassenaar, L.I., Aravena, R., Fritz, P., 1989. The geochemistry and evolution of natural organic solutes in groundwater. Radiocarbon 31 (3), 865–876.
Wendt, I., 1971. Carbon and oxygen isotope exchange between HCO3 in saline solution and solid CaCO3. Earth Planet. Sci. Lett. 12 (4), 439–442.
Whitaker, F.F., Smart, P.L., 1997. Climatic control of hydraulic conductivity of Bahamian limestones. Ground Water 35 (5), 859–868.
Wigley, T., Plummer, L., Pearson, F., 1978. Mass transfer and carbon isotope evolution in natural water systems. Geochim. Cosmochim. Acta 42 (8), 1117–1139.
Yamanaka, M., Kumagai, Y., 2006. Sulfur isotope constraint on the provenance of salinity in a confined aquifer system of the southwestern Nobi Plain, central Japan. J. Hydrol. 325 (1), 35–55.
Yechieli, Y., Kafri, U., Sivan, O., 2009. The inter-relationship between coastal sub-aquifers and the Mediterranean Sea, deduced from radioactive isotopes analysis. Hydrogeol. J. 17 (2), 265–274.
Yechieli, Y., Sivan, O., Lazar, B., Vengosh, A., Ronen, D., Herut, B., 2001. Radiocarbon in seawater intruding into the Israeli Mediterranean coastal aquifer. Radiocarbon 43 (2B), 773–781.